

# Quantum Theory of Phonon Induced Anomalous Hall Effect in 2D Massive Dirac metals

Jia-Xing Zhang<sup>1</sup> and Wei Chen<sup>1,2\*</sup>

<sup>1</sup>*National Laboratory of Solid State Microstructures and School of Physics, Nanjing University, Nanjing, China and*

<sup>2</sup>*Collaborative Innovation Center of Advanced Microstructures, Nanjing University, Nanjing, China*

The phonon induced anomalous Hall or thermal Hall effects have been observed in various systems in recent experiments. However, the theoretical studies on this subject are very scarce and incomplete. In this work, we present a systematic quantum field theory study on the phonon induced anomalous Hall effect, including both the side jump and skew scattering contributions, in a 2D massive Dirac metal, which is considered as the minimum anomalous Hall system. We reveal significant difference from the anomalous Hall effect induced by the widely studied Gaussian disorder which is known to be insensitive to temperature. While the anomalous Hall effect induced by phonon approaches that by Gaussian disorder at high temperature, it behaves very differently at low temperature. Our work provides a microscopic and quantitative description of the crossover from the low to high temperature regime of the phonon induced anomalous Hall conductivity, which may be observed in 2D Dirac metals with breaking time reversal symmetry.

The anomalous Hall effect (AHE), a transverse voltage arising in a metal or semiconductor in response to an applied current without magnetic field, was experimentally discovered as early as 1881 [1]. Ever since then, the search for the microscopic origin of the AHE has been one of the main issues of condensed matter physics [2–12]. The subsequent discoveries have brought the important aspect of topology to modern condensed matter physics [13, 14] and led to many important applications. After a long-lasting debate, it is established that there are two types of mechanisms which may result in AHE in materials with broken time reversal symmetry [10–12]: One is the intrinsic contribution which comes from the nontrivial Berry curvature of the band structure; the other is the extrinsic contribution which originates from electron scatterings by impurities in materials with (pseudo-)spin-orbit interaction. The latter can be further divided to the side jump contribution, which is due to transverse coordinate shift by scatterings, and the skew scattering contributions, which is due to asymmetric scattering [10].

Most previous studies on the extrinsic contribution have focused on electron scatterings off static disorder [9–12, 15, 16]. However, recent experiments have detected various anomalous Hall or thermal Hall effects dominated by electron scatterings off phonons [17, 18]. Yet the theoretical studies of the phonon-induced AHE are very scarce and incomplete so far. In [19], the authors present a semiclassical Boltzmann equation (SBE) approach for the phonon induced side jump conductivity in 2D massive Dirac model, however it is a difficult task to generalize this approach to the phonon induced skew scattering contribution, the study of which is absent so far. On the other hand, a couple of early works tried to study the AHE due to e-phonon interaction in 2D Rashba ferromagnets in a full quantum field theory approach [20, 21]. However, these works were done long before the microscopic mechanisms of the AHE were well

understood. For the reason, they are still far from being complete and transparent.

In this work we present a unified and systematic quantum field theory study of the extrinsic AHE due to phonon scatterings in a 2D massive Dirac metal, which is considered as a minimum anomalous Hall (AH) system [10, 16]. For simplicity, we focus on the scalar phonon mode, or the deformation potential (DP) induced AHE in this system. We obtained the AH conductivity, including both the side jump and skew scattering contributions due to phonon scatterings in the temperature range  $T \ll \epsilon_F$ , as plotted in Fig.2. The analytic results of the AH conductivities in the limit  $T \ll T_{BG}$  and  $T \gg T_{BG}$ , where  $T_{BG} \equiv 2sk_F$  is the Bloch-Gruneisen temperature, are shown in Table I. Compared to the widely studied AHE induced by Gaussian disorder, we reveal significant difference in the phonon induced AHE: (a) While the disorder induced AHE is insensitive to temperature, the phonon induced AHE depends on temperature significantly. Only at the high temperature limit  $T \gg T_{BG}$ , the unscreened DP induced AHE saturates to the AHE induced by Gaussian disorder. (b) While the side jump contribution due to phonon scatterings is finite as  $T$  goes to zero, the phonon induced skew scattering contribution (with the non-crossing approximation) approaches zero as  $\sim T^2$  when the temperature  $T$  goes to zero. This is in significant difference from the AHE induced by Gaussian disorder in a 2D massive Dirac metal, for which both the side jump and skew scattering contributions are finite as  $\sim T^0$  in the whole temperature range.

We start with a 2D massive Dirac model with

$$\mathcal{H}_0 = v\boldsymbol{\sigma} \cdot \mathbf{k} + \Delta\sigma_z \quad (1)$$

where  $\boldsymbol{\sigma} = (\sigma_x, \sigma_y)$  is composed of Pauli matrices and  $\Delta$  is the mass of the Dirac fermion which breaks the time reversal symmetry of  $\mathcal{H}_0$ . The two energy bands of  $\mathcal{H}_0$  are  $\epsilon_k^\pm = \pm\sqrt{v^2k^2 + \Delta^2}$ . The corresponding

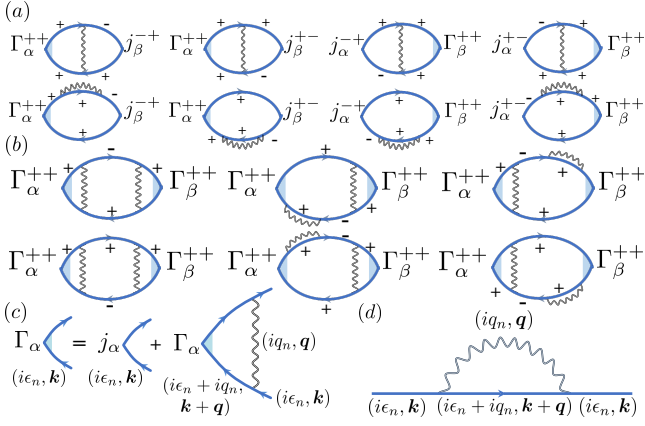


FIG. 1: The Feynman diagrams of phonon induced (a) side jump and (b) skew scattering contributions. The solid and curvy lines represent the electron and phonon propagators respectively. The + and - label the propagators of the upper and lower band electrons respectively. (c) The depiction of the recursion equation of the renormalized current vertex. (d) The electron self-energy in the first Born approximation.

eigenstates are  $|\mathbf{k}, +\rangle = (\cos \frac{\alpha}{2}, \sin \frac{\alpha}{2} e^{i\theta_0})^T$  and  $|\mathbf{k}, -\rangle = (\sin \frac{\alpha}{2}, -\cos \frac{\alpha}{2} e^{i\theta_0})^T$  where  $\cos \alpha \equiv \Delta/|\epsilon_k^\pm|$  and  $\theta_0$  is the polar angle of  $\mathbf{k}$ .

The electron-phonon interaction can be written as

$$\mathcal{H}_{ep} = \sum_{\mathbf{k}, \mathbf{q}} \hat{\Psi}_{\mathbf{k}+\mathbf{q}}^\dagger \hat{M}(\mathbf{q}) \hat{\Psi}_{\mathbf{k}} (\hat{b}_{\mathbf{q}} + \hat{b}_{-\mathbf{q}}^\dagger), \quad (2)$$

where  $\hat{\Psi}_{\mathbf{k}}$  and  $\hat{b}_{\mathbf{q}}$  represent the electron and phonon field respectively. For simplicity, in this work we focus on the AHE induced by acoustic DP for which the e-phonon interaction vertex can be written as a scalar as  $\hat{M}_{DP}(\mathbf{q}) = g_{\mathbf{q}} \equiv iq\xi_q g_D$ , where  $\xi_q \equiv \sqrt{1/2\rho\omega_{\mathbf{q}}}$ ,  $\omega_{\mathbf{q}} \approx sq$  is the phonon frequency,  $\rho$  is the atomic mass density and  $g_D$  is the DP strength. We ignore the screening effect on the DP at first and discuss its correction at the end of the calculation.

We set the electron Fermi energy  $\epsilon_F > 0$  as the largest energy scale in this work, i.e.,  $\epsilon_F \gg T, T_{BG}$ . The phonon scattering induced AHE can be obtained by treating the phonons as impurities excited by the temperature. We assume weak e-phonon interaction such that  $\epsilon_F \tau \gg 1$  where  $\tau$  is the mean lifetime of electrons. The AH conductivity is a sum of two contributions  $\sigma_{xy} = \sigma_{xy}^I + \sigma_{xy}^{II}$  using the Kubo-Streda formula [7, 10]. The quantity  $\sigma_{xy}^I$  may be considered as a contribution from electrons on the Fermi surface whereas  $\sigma_{xy}^{II}$  is determined by all electron states under the Fermi surface. Since  $\sigma^{II}$  is insensitive to impurity scatterings at  $\epsilon_F \tau \gg 1$  [10], we focus on the study of  $\sigma_{xy}^I$  which can be written as

$$\sigma_{xy}^I = - \sum_{\mathbf{k}} \int \frac{d\epsilon}{2\pi} \partial_\epsilon n_F(\epsilon) \text{Tr}[\hat{\Gamma}_x G^R(\epsilon, \mathbf{k}) \hat{j}_y G^A(\epsilon, \mathbf{k})], \quad (3)$$

where  $G^{R/A}$  is the retarded/advanced electron Green's function (GF), and  $\hat{j}_y$  and  $\hat{\Gamma}_x$  are the bare and renormalized current vertex respectively.

The phonon induced side jump and skew scattering contributions can be most easily separated from  $\sigma_{xy}^I$  by expanding the trace in Eq.(3) in the eigenstate band basis [10, 23]. The results are depicted in Fig.1(a) and (b).

The phonon propagator in the imaginary time formalism is

$$D_0(iq_n, \mathbf{q}) \equiv -\langle T_\tau u_{\mathbf{q}} u_{-\mathbf{q}} \rangle = \frac{2\omega_{\mathbf{q}}}{(iq_n)^2 - \omega_{\mathbf{q}}^2}, \quad (4)$$

where  $u_{\mathbf{q}} \equiv b_{\mathbf{q}} + b_{-\mathbf{q}}^\dagger$  and  $iq_n = 2n\pi i/\beta$ ,  $n \in Z$  is the phonon Matsubara frequency. Here we do not include the phonon self-energy due to e-phonon interaction explicitly because it only results in a renormalisation of the phonon velocity  $s$ . Therefore we only need to assume the phonon velocity is the renormalized one.

The leading order contribution to the AHE requires the electron GF in the first Born approximation  $G(i\epsilon_n, \mathbf{k}) = [i\epsilon_n - \mathcal{H}_0 - \Sigma(i\epsilon_n, \mathbf{k})]^{-1}$  [10, 23], where the electron self-energy  $\Sigma(i\epsilon_n, \mathbf{k})$  due to e-phonon interaction is depicted in Fig.1(d). Since the phonon energy is much smaller than the electron Fermi energy  $\epsilon_F$ , we make the approximation that the electrons are bound to the Fermi surface both before and after the scattering with a phonon, i.e., the scatterings are quasi-elastic. The inclusion of the energy transfer during the scatterings only results in a correction smaller in the order of  $T_{BG}/\epsilon_F$  in the AH conductivity. With this approximation, we obtain the electron self-energy after analytic continuation to the real energy axis as [22]

$$\Sigma^R(\epsilon, \mathbf{k}) \approx -\frac{i}{2} [a(1 + \frac{\Delta}{\epsilon} \sigma_z) + v \frac{b}{\epsilon} \boldsymbol{\sigma} \cdot \mathbf{k}]. \quad (5)$$

The full expressions of the parameters  $a, b$  are given in the supplemental materials (SM) [22]. It is hard to work out  $a$  and  $b$  analytically in the whole temperature regime, but we can obtain their analytical results in the  $T \ll T_{BG}$  and  $T \gg T_{BG}$  limits, as shown in Table I.

The Feynman diagrams for the AH conductivity include a vertex correction to the current operator by the e-phonon interaction, as shown in Fig.1(c). The leading order current vertex correction involves scatterings only within the upper electron band and the vertex correction due to such scatterings needs to be summed to infinite order [10]. Instead, for the vertex correction due to inter-band scatterings, only the lowest order needs to be kept in the calculation of the AH conductivity. The renormalized diagonal matrix element of the current vertex in the dc limit associated with the upper band, i.e.,  $\Gamma_\alpha^{++}(\epsilon, \epsilon; \mathbf{k}) \equiv \langle \mathbf{k}, + | \hat{\Gamma}_\alpha(\epsilon, \epsilon; \mathbf{k}) | \mathbf{k}, + \rangle$ ,  $\alpha = x, y$ , satisfies

	$T \ll T_{BG}$	$T \gg T_{BG}$
$\sigma_{xy}^{\text{side}}$	$-\frac{e^2}{4\pi} \frac{\Delta}{\epsilon_F} (1 - \frac{\Delta^2}{\epsilon_F^2})$	$-\frac{e^2}{\pi} \frac{\Delta}{\epsilon_F} \frac{v^2 k_F^2}{\epsilon_F^2 + 3\Delta^2}$
$\sigma_{xy}^{\text{sk-nc}}$	$-\frac{\pi e^2}{2} \frac{\Delta}{\epsilon_F} (1 - \frac{\Delta^2}{\epsilon_F^2})^2 \frac{T^2}{T_{BG}^2}$	$-\frac{3e^2}{4\pi} \frac{\Delta}{\epsilon_F} (\frac{v^2 k_F^2}{\epsilon_F^2 + 3\Delta^2})^2$
a	$\frac{\pi^2}{4} C (1 + \frac{\pi^2}{4} t^2 + \frac{3}{8} \pi^4 t^4)$	$\frac{\pi}{2} C (1/t - \frac{1}{12} t)$
b	$\frac{\pi^2}{4} C (1 - \frac{3\pi^2}{4} t^2 - \frac{5}{8} \pi^4 t^4)$	$\frac{\pi}{48} C/t^3$
c	$\frac{\pi^2}{4} C (1 - \frac{7\pi^2}{4} t^2 + \frac{19}{8} \pi^4 t^4)$	$\frac{\pi}{4} C (1/t - \frac{1}{12} t)$

TABLE I: The parameters  $a, b, c$  and the leading order AH conductivities at the low and high temperature limit without screening, where  $C \equiv \frac{1}{2\pi} \frac{g_D^2}{\rho v^2 s^3} \frac{\epsilon_F}{k_F} (k_B T)^2$ ,  $t \equiv T/T_{BG}$  and we set  $\hbar = 1$ .

the recursion equation [22]

$$\Gamma_{\alpha}^{++}(\epsilon, \epsilon; \mathbf{k}) = j_{\alpha}^{++}(\mathbf{k}) + \sum_{\mathbf{q}} \int d\xi |g_{\mathbf{q}}|^2 |\langle \mathbf{k} + \mathbf{q}, + | \mathbf{k}, + \rangle|^2$$

$$G^{R+}(\xi, \mathbf{k} + \mathbf{q}) G^{A+}(\xi, \mathbf{k} + \mathbf{q}) \Gamma_{\alpha}^{++}(\xi, \xi; \mathbf{k} + \mathbf{q})$$

$$[\delta(\xi - \epsilon - \omega_{\mathbf{q}})(n_B(\omega_{\mathbf{q}}) + n_F(\xi))$$

$$+ \delta(\xi - \epsilon + \omega_{\mathbf{q}})(n_B(\omega_{\mathbf{q}}) + 1 - n_F(\xi))], \quad (6)$$

where  $j_{\alpha}^{++}(\mathbf{k}) = \langle \mathbf{k}, + | e v \sigma_{\alpha} | \mathbf{k}, + \rangle = e v \frac{v k_{\alpha}}{\epsilon_k}$  is the bare current matrix element and

$$G^{R/A,+}(\epsilon, \mathbf{k}) = \langle \mathbf{k}, + | G^{R/A} | \mathbf{k}, + \rangle = \frac{1}{\epsilon - \epsilon_k^+ \pm \frac{i}{2\tau_k^+}} \quad (7)$$

are the retarded and advanced GF of the upper band electrons. The upper band scattering rate is

$$1/\tau_k^+ = (1 + \frac{\Delta^2}{\epsilon \epsilon_k}) a + \frac{v^2 k^2}{\epsilon \epsilon_k} b. \quad (8)$$

The recursion Eq.(6) is hard to solve exactly. But with the quasi-elastic scattering approximation, we can obtain the renormalized current vertex element  $\Gamma_{\alpha}^{++}$  by an order by order iteration of Eq.(6) followed by a sum over all the orders. We get the renormalized current vertex as [22]

$$\Gamma_{\alpha}^{++}(\epsilon, \epsilon; \mathbf{k}) = \gamma \frac{e v^2 k_{\alpha}}{\epsilon}, \quad (9)$$

$$\gamma = \frac{1}{1 - \lambda}, \quad \lambda = \frac{b + c + \frac{\Delta^2}{\epsilon^2}(b - c)}{a + b + \frac{\Delta^2}{\epsilon^2}(a - b)}, \quad (10)$$

where the full expression of the new parameter  $c$  is given in the SM [22] and its result at low and high temperature is shown in Table I. It is interesting to note that the vertex correction factor  $\gamma$  we obtained above from Eq.(6) is equal to  $\tilde{\tau}_k^{tr}/\tau_k^+$ , where  $\tilde{\tau}_k^{tr}$  and  $\tau_k^+$  are respectively the modified transport and mean lifetime of the upper band electrons with phonon scatterings defined in [19, 22].

In the low and high temperature limit, by expanding the parameters  $a, b$  and  $c$ , as shown in Table I, we obtain

$$\gamma \approx \frac{1}{\pi^2} \left( \frac{T_{BG}}{T} \right)^2 \left[ 1 + \frac{3\pi^2}{4} (1 - 2 \frac{\Delta^2}{\epsilon_F^2}) \left( \frac{T}{T_{BG}} \right)^2 \right] \quad (11)$$

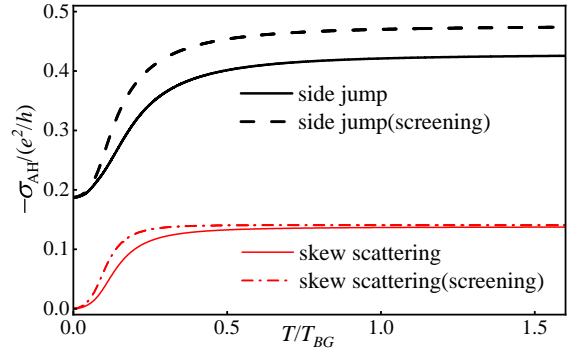


FIG. 2: The side jump and skew scattering conductivities as a function of  $t = T/T_{BG}$  for  $\Delta/\epsilon_F = 1/2$  and  $\alpha = 2$ . The dashed and solid lines represent the results with and without the screening effect respectively.

at  $T \ll T_{BG}$  and

$$\gamma \approx 2 \frac{\epsilon_F^2 + \Delta^2}{\epsilon_F^2 + 3\Delta^2} + \frac{1}{12} \left( \frac{T_{BG}}{T} \right)^2 \frac{\epsilon_F^4 + \Delta^4 + 6\epsilon_F^2 \Delta^2}{(\epsilon_F^2 + 3\Delta^2)^2} \quad (12)$$

at  $T \gg T_{BG}$ . It seems unusual that  $\gamma$  diverges as  $\sim 1/T^2$  when  $T \rightarrow 0$ . This is because both  $1/\tau_k^+$  and  $1/\tilde{\tau}_k^{tr}$  vanish as a power law of  $T$  when  $T \rightarrow 0$ , but the transport scattering rate  $1/\tilde{\tau}_k^{tr}$  vanishes faster than  $1/\tau_k^+$ . We will see later that this divergence of  $\gamma$  at  $T \rightarrow 0$  does not lead to the divergence of the AH conductivity at  $T \rightarrow 0$ . At high temperature  $T \gg T_{BG}$ ,  $\gamma$  reduces to  $2 \frac{\epsilon_F^2 + \Delta^2}{\epsilon_F^2 + 3\Delta^2}$ , which is the same as the current vertex renormalization factor by Gaussian disorder [10].

With the above ingredients, we can compute the side jump and skew scattering contributions due to phonon scatterings depicted in Fig.1(a) and (b). After a lengthy calculation [22], we obtain the two AH conductivities in the dc limit in a 2D massive Dirac metal as

$$\sigma_{xy}^{\text{side}} = -\frac{e^2}{2\pi} \frac{\Delta}{\epsilon_F} \left( 1 - \frac{\Delta^2}{\epsilon_F^2} \right) \frac{(a - b)}{a - c + \frac{\Delta^2}{\epsilon_F} (a + c - 2b)}, \quad (13)$$

$$\sigma_{xy}^{\text{sk-nc}} = -\frac{e^2 \Delta}{4\pi \epsilon_F} \left( 1 - \frac{\Delta^2}{\epsilon_F^2} \right)^2 \frac{(a + c - 2b)(a - c)}{[a - c + \frac{\Delta^2}{\epsilon_F} (a + c - 2b)]^2}. \quad (14)$$

Equations (13)-(14) are the main results of this work. From the expressions of  $a, b, c$  in the SM [22], we can see that both  $\sigma_{xy}^{\text{side}}$  and  $\sigma_{xy}^{\text{sk-nc}}$  scale as a function of  $t \equiv T/T_{BG}$ . The scaling functions  $\sigma_{xy}^{\text{side}}(t)$  and  $\sigma_{xy}^{\text{sk-nc}}(t)$  only depend on  $\Delta/\epsilon_F$  and  $t$ . The numerical plots of  $\sigma_{xy}^{\text{side}}(t)$  and  $\sigma_{xy}^{\text{sk-nc}}(t)$  as a function of  $t = T/T_{BG}$  for a given  $\Delta/\epsilon_F = 1/2$  are shown in Fig.2.

Table I shows the analytical results of the side jump and skew scattering contributions in the limits  $T \ll T_{BG}$  and  $T \gg T_{BG}$ . At  $T \gg T_{BG}$ , both the side jump and skew scattering conductivities approach the values induced by Gaussian disorder in [10], indicating the

saturation of phonon scatterings in this limit. At low temperature, however, the AH conductivity induced by deformation potential is significantly different from that induced by Gaussian disorder.

At  $T \ll T_{BG}$ , we obtain the side jump contribution due to phonon scatterings as

$$\sigma_{xy}^{\text{side}} \approx -\frac{e^2}{4\pi\epsilon_F} \left(1 - \frac{\Delta^2}{\epsilon_F^2}\right) \left[1 + 2\pi^2 \left(1 - \frac{\Delta^2}{\epsilon_F^2}\right) \left(\frac{T}{T_{BG}}\right)^2\right]. \quad (15)$$

This result is consistent with the side jump contribution at  $T \rightarrow 0$  obtained from the SBE approach for phonon scatterings in [19], but different from the result due to Gaussian disorder in [10].

For the phonon induced skew scattering contribution, the expansion of  $a, b, c$  at  $T \ll T_{BG}$  in Table I gives

$$\sigma_{xy}^{\text{sk-nc}} = -\frac{\pi e^2}{2\epsilon_F} \left(1 - \frac{\Delta^2}{\epsilon_F^2}\right)^2 \frac{T^2}{T_{BG}^2} + \mathcal{O}[(T/T_{BG})^4], \quad (16)$$

i.e., the skew scattering contribution approaches zero as  $\sim (T/T_{BG})^2$  at  $T \rightarrow 0$ , as can be also seen from the numerical plot in Fig.2. This is significantly different from the skew scattering contribution induced by Gaussian disorder with the noncrossing approximation, which is finite as  $T \rightarrow 0$ .

The above calculation ignored the screening effects by the electrons. To take into account this effect, we add the Thomas-Fermi (TF) screening factor to the deformation potential by replacing  $g_D$  with  $g_D \frac{q}{q+q_{TF}}$ , where  $q_{TF} \sim \alpha\epsilon_F/v$  is the TF wave vector and  $\alpha = e^2/\hbar v$  is the fine structure constant [24, 25]. The AH conductivities including the screening effect are plotted in Fig.2 (for which we set  $\alpha = 2$  as for graphene). One can see that the inclusion of screening does not change the AH conductivities at  $T \rightarrow 0$ . Particularly, for the skew scattering contribution,  $\sigma_{xy}^{\text{sk-nc}}$  still vanishes as  $\sim T^2/T_{BG}^2$  at  $T \rightarrow 0$  but with a modified coefficient as  $\tilde{\sigma}_{xy}^{\text{sk-nc}} \approx \frac{17}{8}\sigma_{xy}^{\text{sk-nc}}$ . At finite temperature, the screening effect modifies the AH conductivities and their limiting values at  $T \gg T_{BG}$  depend on  $\alpha$ . More detailed discussion of the screening effect is shown in [22].

The temperature dependence of the phonon induced side-jump conductivity has been pointed out in previous works with the semi-classical approach [19, 26]. This is in contrast to the AHE due to Gaussian disorder for which the AH conductivity is independent of the temperature. The reason is because the AH conductivity depends on the scattering range [29], which depends on the temperature  $T$  for phonon scatterings [19, 26] but independent of  $T$  for Gaussian disorder. At  $T \gg T_{BG}$ , the phonons participating in the scatterings saturate and the momentum transfer during the scatterings is randomly distributed from 0 to  $2k_F$ . The average momentum transfer, or the scattering range then approaches that for Gaussian disorder in [10], so does the AH conductivity. The quantum approach in this work

provides a microscopic and quantitative description of the crossover from the low to high temperature of the AH conductivity due to phonon scatterings.

It is worth noting that the Feynman diagrams with two crossed impurity lines were shown to contribute the same order to the AH conductivity as the non-crossing diagrams for Gaussian disorder in recent years [27–31]. For the phonon induced AHE, we can not exclude the importance of such diagrams either. However, due to the complexity of the calculation and the limited space, we leave the study of these diagrams for a future work.

The phonon induced AHE and its temperature dependence we discussed above may be observed in clean 2D Dirac metals with TRS breaking, such as  $\text{Fe}_3\text{Sn}_2$ , which is a quasi-2D ferromagnetic Dirac metal [32], or graphene with spin-orbit interaction and TRS breaking [16]. The spin-orbit interaction results in a gap or finite mass in the graphene. The TRS breaking avoids the cancellation of the AH conductivities from the two valleys and may be achieved by spin polarization of the graphene through optical orientation [33], or ferromagnetic contacts [16].

*Acknowledgement.* This work is supported by the NNSF of China under Grant No.11974166 and the Department of Science and Technology of Jiangsu Province under Grant No. BK20231398.

---

\* Electronic address: chenweiphy@nju.edu.cn

- [1] E. Hall, Philos. Mag. **12**, 157 (1881).
- [2] J. Smit, Physica Amsterdam **21**, 877(1955).
- [3] J. M. Luttinger and W. Kohn, Phys. Rev. **97**, 869(1955).
- [4] J. M. Luttinger, Phys. Rev. **112**, 739(1958).
- [5] R. Karplus and J. M. Luttinger, Phys. Rev. **95**, 1154(1964).
- [6] L. Berger, Phys. Rev. B **2**, 4559(1970).
- [7] P. Streda, J. Phys. C **15**, L717(1982).
- [8] R. Shindou, and L. Balents, Phys. Rev. Lett. **97**, 216601(2006).
- [9] N. A. Sinitsyn, Q. Niu, and A. H. MacDonald, Phys. Rev. B **73**, 075318(2006).
- [10] N. A. Sinitsyn, A. H. MacDonald, T. Jungwirth, V. K. Dugaev, and J. Sinova, Phys. Rev. B **75**, 045315(2007).
- [11] N. A. Sinitsyn, J. Phys.: Cond. Matt. **20**, 023201(2008).
- [12] N. Nagaosa, J. Sinova, S. Onoda, A. H. MacDonald, and N. P. Ong, Rev. Mod. Phys. **82**, 1539(2010).
- [13] F. D. M. Haldane, Phys. Rev. Lett. **93**, 206602(2004).
- [14] D. Xiao, M. C. Chang, and Q. Niu, Rev. Mod. Phys. **82**, 1959(2010).
- [15] S. Yang, H. Pan, Y. Yao, and Q. Niu, Phys. Rev. B **83**, 125122(2011).
- [16] N. A. Sinitsyn, J. E. Hill, H. Min, J. Sinova, and A. H. MacDonald, Phys. Rev. Lett. **97**, 106804(2006).
- [17] J. Duan, Y. Jian, Y. Gao, H. Peng, J. Zhong, Q. Feng, J. Mao, and Y. Yao, Phys. Rev. Lett. **129**, 186801(2022).
- [18] R. Sharma, M. Bagchi, Y. Wang, Y. Ando, and T. Lorenz, arXiv:2401.03064.
- [19] C. Xiao, Y. Liu, M. Xie, S.Y. A. Yang, and Q. Niu, Phys. Rev. B **99**, 245418(2019).

- [20] H. R. Leribaux, Phys. Rev. **150**, 384 (1966).
- [21] S. K. Lyo, Phys. Rev. B **8**, 1185 (1973).
- [22] See the supplemental materials of this manuscript.
- [23] J. X. Zhang, Z. Y. Wang, and W. Chen, Phys. Rev. B **107**, 125106(2023).
- [24] W. Chen and A. A. Clerk, Phys. Rev. B **86**, 125443(2012).
- [25] E. Mariani and F. von Oppen, Phys. Rev. B **82**, 195403(2010).
- [26] C. Xiao, Y. Liu, Z. Yuan, S. Y. A. Yang, and Q. Niu, Phys. Rev. B **100**, 085425(2019).
- [27] I. A. Ado, I. A. Dmitriev, P. M. Ostrovsky, and M. Titov, Europhys. Lett. **111**, 37004 (2015).
- [28] I. A. Ado, I. A. Dmitriev, P. M. Ostrovsky, and M. Titov, Phys.Rev. Lett. **117**, 046601(2016).
- [29] I. A. Ado, I. A. Dmitriev, P. M. Ostrovsky, and M. Titov, Phys. Rev. B **96**, 235148 (2017).
- [30] E. J. Konig and A. Levchenko, Phys. Rev. Lett. **118**, 027001(2017).
- [31] J. X. Zhang, and W. Chen, Phys. Rev. B **107**, 214204(2023).
- [32] M. Papaj, and L. Fu, Phys. Rev. B **103**, 075424(2021).
- [33] V. I. Belinicher and B. I. Sturman, Usp. Fiz. Nauk **130**, 415 (1980) [Sov. Phys. Usp. **23**, 199 (1980)].

## SUPPLEMENTAL MATERIALS

### I. ELECTRON SELF-ENERGY AND GREEN'S FUNCTION IN THE FIRST BORN APPROXIMATION

#### A. Electron Self-energy

We show the detailed calculation of the electron self-energy due to the e-phonon interaction and the electron Green's function (GF) in the first Born approximation in this section.

The Hamiltonian of a 2D massive Dirac model is shown in the main text as

$$\mathcal{H}_0 = v\mathbf{k} \cdot \boldsymbol{\sigma} + \Delta\sigma_z. \quad (17)$$

The two energy bands of  $\mathcal{H}_0$  are  $\epsilon_k^\pm = \pm\epsilon_k$ ,  $\epsilon_k = \sqrt{v^2k^2 + \Delta^2}$  and the two eigenstates are  $|\mathbf{k}, +\rangle = (\cos \frac{\alpha}{2}, \sin \frac{\alpha}{2} e^{i\theta_0})^T$  and  $|\mathbf{k}, -\rangle = (\sin \frac{\alpha}{2}, -\cos \frac{\alpha}{2} e^{i\theta_0})^T$  where  $\cos \alpha \equiv \Delta/\epsilon_k$  and  $\theta_0$  is the polar angle of  $\mathbf{k}$ , as shown in Fig.3(c). The bare electron Matsubara GF is

$$G_0(i\epsilon_n, \mathbf{k}) = \frac{1}{(i\epsilon_n)^2 - \epsilon_k^2} (i\epsilon_n\sigma_0 + \Delta\sigma_z + v\mathbf{k} \cdot \boldsymbol{\sigma}), \quad (18)$$

where  $i\epsilon_n = (2n+1)\pi i/\beta$  is the electron Matsubara frequency with  $\beta = 1/k_B T$ ,  $n \in Z$ .

The electron-phonon interaction for acoustic deformation potential (DP) has been given in the main text as

$$\mathcal{H}_{ep} = \sum_{\mathbf{k}, \mathbf{q}} \hat{\Psi}_{\mathbf{k}+\mathbf{q}}^\dagger g_{\mathbf{q}} \hat{\Psi}_{\mathbf{k}} (\hat{b}_{\mathbf{q}} + \hat{b}_{-\mathbf{q}}^\dagger), \quad (19)$$

where  $\hat{\Psi}_{\mathbf{k}}$  and  $\hat{b}_{\mathbf{q}}$  represent the electron and the phonon fields respectively. The coupling constant  $g_{\mathbf{q}} \equiv iq\xi_q g_D$ , where  $\xi_q \equiv \sqrt{1/2\rho\omega_{\mathbf{q}}}$ ,  $\omega_{\mathbf{q}} \approx sq$  and  $g_D$  is the DP strength. We set  $\hbar = 1$  for convenience in the whole text.

The Feynman diagram of the electron self-energy is shown in Fig.3a. The solid line represents the electron GF and the curvy line represents the phonon GF

$$D_0(iq_n, \mathbf{q}) \equiv -\langle T_\tau u_{\mathbf{q}} u_{-\mathbf{q}} \rangle = \frac{2\omega_{\mathbf{q}}}{(iq_n)^2 - \omega_{\mathbf{q}}^2}, \quad (20)$$

where  $u_{\mathbf{q}} \equiv b_{\mathbf{q}} + b_{-\mathbf{q}}^\dagger$  and  $iq_n = 2n\pi i/\beta$ ,  $n \in Z$  is the phonon Matsubara frequency.

The electron self-energy in the first Born approximation can be expressed as

$$\Sigma(i\epsilon_n, \mathbf{k}) = -\frac{1}{\beta} \sum_{iq_n} \sum_{\mathbf{q}} |g_{\mathbf{q}}|^2 D_0(iq_n, \mathbf{q}) G_0(i\epsilon_n + iq_n, \mathbf{k} + \mathbf{q}). \quad (21)$$

The sum over the phonon Matsubara frequency  $iq_n$  may be obtained by performing the following integral over the contour in Fig.3b:

$$\begin{aligned} & \int_C \frac{dz}{2\pi i} n_B(z) D_0(z, \mathbf{q}) G_0(z + i\epsilon_n, \mathbf{k} + \mathbf{q}) \\ &= \int_{-\infty}^{\infty} \frac{d\xi}{2\pi i} n_B(\xi - i\epsilon_n) D_0(\xi - i\epsilon_n, \mathbf{q}) [G_0(\xi + i0^+, \mathbf{k} + \mathbf{q}) - G_0(\xi - i0^+, \mathbf{k} + \mathbf{q})] \\ &= \frac{1}{\beta} \sum_{iq_n} D_0(iq_n, \mathbf{q}) G_0(iq_n + i\epsilon_n, \mathbf{k} + \mathbf{q}) + \sum_{z_j = \pm\omega_q} \text{Res}[D_0(z = z_j, \mathbf{q})] G_0(z_j + i\epsilon_n, \mathbf{k} + \mathbf{q}) n_B(z_j), \end{aligned} \quad (22)$$

where  $n_B(z)$  is the Bose-Einstein distribution function and  $\text{Res}[D_0(z = z_j, \mathbf{q})]$  is the residue of  $D_0(z, \mathbf{q})$  at  $z = z_j$ .

We assume that the e-phonon interaction is weak so the real part of the self energy is much smaller than the Fermi energy and we can ignore it. We then only need to compute the imaginary part of the electron self-energy. From Eq.(22), we obtain the self-energy (i.e., imaginary part) after the sum over the Matsubara frequency  $iq_n$  and the analytic continuation  $i\epsilon_n \rightarrow \epsilon + i0^+$  to real energy axis as

$$\Sigma^R(\epsilon, \mathbf{k}) = (-i\pi) \sum_{\mathbf{q}} |g_{\mathbf{q}}|^2 \int_{-\infty}^{\infty} \frac{d\xi}{2\xi} \delta(\xi - \epsilon_{\mathbf{k}+\mathbf{q}}) [\xi\sigma_0 + \Delta\sigma_z + v(\mathbf{k} + \mathbf{q}) \cdot \boldsymbol{\sigma}] \quad (23)$$

$$\times [\delta(\xi - \epsilon - \omega_q)(n_B(\omega_q) + n_F(\xi)) - \delta(\xi - \epsilon + \omega_q)(n_B(-\omega_q) + n_F(\xi))], \quad (24)$$

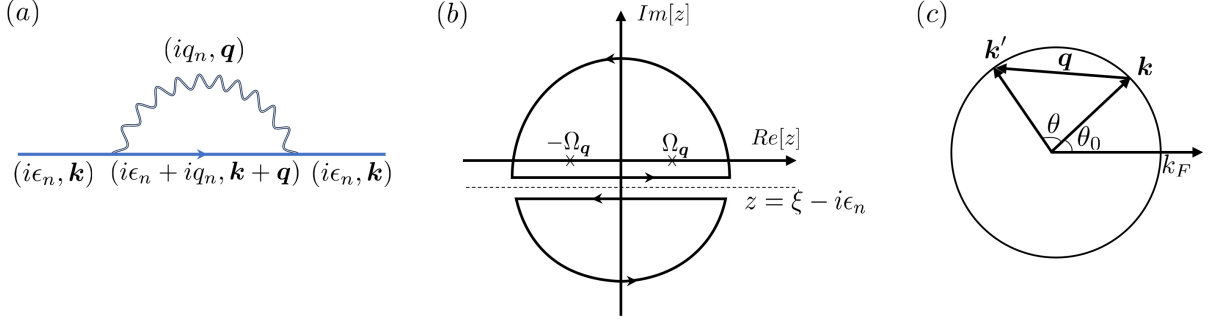


FIG. 3: (a) Feynman diagram of the electron self-energy due to e-phonon interaction. The solid and curvy lines represent the electron and phonon propagators respectively. (b) The integration contour for the summation of the phonon Matsubara frequency of the self-energy. (c) Quasi-elastic scattering of an electron off a phonon near the Fermi surface. Here  $\mathbf{k}$  and  $\mathbf{k}'$  are the initial and final momentum of the electron and  $\mathbf{q}$  is the momentum of the phonon.

where  $n_F(\xi)$  is the Fermi-Dirac distribution function and we have used  $n_B(\xi - i\epsilon_n) = -n_F(\xi)$ .

For an electron with momentum  $\mathbf{k}$  on the Fermi surface, and the phonon energy  $\omega_q$  much smaller than the Fermi energy  $\epsilon_F$ , the electron after scattering with a phonon is still very close to the Fermi surface so the maximum momentum (energy) of the phonon participating in the scatterings is about  $2k_F$  ( $2sk_F$ ). The sum over the phonon momentum  $\mathbf{q}$  in the self-energy may be converted to the integral over  $\mathbf{k}' = \mathbf{k} + \mathbf{q}$  as

$$\begin{aligned} \Sigma^R(\epsilon, \mathbf{k}) = & \frac{(-i\pi)}{(2\pi)^2} \frac{g_D^2}{2\rho s^2} \int_{-\infty}^{\infty} \frac{d\xi}{2\xi} \int_0^{k_B T_{BG}} \Omega d\Omega \\ & [\delta(\xi - \epsilon - \Omega)(n_B(\Omega) + n_F(\xi)) + \delta(\xi - \epsilon + \Omega)(n_B(\Omega) + 1 - n_F(\xi))] \\ & \int_0^{2\pi} d\theta \delta(\Omega - \omega_q) \int k' dk' \delta(\xi - \epsilon_{\mathbf{k}'}) \times \begin{pmatrix} \xi + \Delta & vk'e^{-i\theta}e^{-i\theta_0} \\ vk'e^{i\theta}e^{i\theta_0} & \xi - \Delta \end{pmatrix}, \end{aligned} \quad (25)$$

where  $\theta_0$  is the polar angle of  $\mathbf{k}$ ,  $\theta$  is the angle between  $\mathbf{k}$  and  $\mathbf{k}'$  and  $\omega_q \approx 2sk \sin \frac{\theta}{2}$ . We have introduced an integration over  $d\Omega$  through the factor  $\delta(\Omega - \omega_q)$  in the above equation. This procedure converts the integration over the angle  $d\theta$  to the integration over  $d\Omega$  through the relationship  $\omega_q \approx 2sk \sin \frac{\theta}{2}$ . Since  $\epsilon_{k'} = \sqrt{v^2 k'^2 + \Delta^2}$ ,  $k' dk' = \frac{\epsilon_{k'}}{v^2} d\epsilon_{k'}$ , the integration over  $k'$  can be converted to  $\epsilon_{k'}$ . After the integration over  $\epsilon_{k'}$  and  $\theta$ , we get

$$\begin{aligned} \Sigma^R(\epsilon, \mathbf{k}) = & -\frac{i}{4\pi} \frac{g_D^2}{2\rho v^2 s^4} \int_0^{k_B T_{BG}} \Omega^2 d\Omega \frac{1}{kp} [1 - (\frac{k^2 + p^2 - (\Omega/s)^2}{2kp})^2]^{-1/2} \\ & \int_{-\infty}^{\infty} d\xi [\delta(\xi - \epsilon - \Omega)(n_B(\Omega) + n_F(\xi)) + \delta(\xi - \epsilon + \Omega)(n_B(\Omega) + 1 - n_F(\xi))] \\ & \begin{pmatrix} \xi + \Delta & vpe^{-i\theta_0} \frac{k^2 + p^2 - (\Omega/s)^2}{2kp} \\ vpe^{i\theta_0} \frac{k^2 + p^2 - (\Omega/s)^2}{2kp} & \xi - \Delta \end{pmatrix}, \end{aligned} \quad (26)$$

where  $p = \frac{\sqrt{\xi^2 - \Delta^2}}{v}$ .

We can write the above self-energy as

$$\Sigma^R(\epsilon, \mathbf{k}) = -\frac{i}{2} \begin{pmatrix} a + \frac{\Delta}{\epsilon} \tilde{a} & v(k_x - ik_y) \frac{b}{\epsilon} \\ v(k_x + ik_y) \frac{b}{\epsilon} & a - \frac{\Delta}{\epsilon} \tilde{a} \end{pmatrix}, \quad (27)$$

where the parameters  $a, \tilde{a}, b$  are

$$\begin{aligned} a(\epsilon, k) = & \frac{1}{4\pi} \frac{g_D^2}{\rho v^2 s^4} \frac{1}{k} \int_{-\infty}^{\infty} d\xi \int_0^{k_B T_{BG}} \Omega^2 d\Omega \frac{1}{p} [1 - (\frac{k^2 + p^2 - (\Omega/s)^2}{2kp})^2]^{-1/2} \\ & \times \xi [\delta(\xi - \epsilon - \Omega)(n_B(\Omega) + n_F(\xi)) + \delta(\xi - \epsilon + \Omega)(n_B(\Omega) + 1 - n_F(\xi))], \end{aligned} \quad (28)$$

$$\begin{aligned} \tilde{a}(\epsilon, k) = & \frac{\epsilon}{4\pi} \frac{g_D^2}{\rho v^2 s^4} \frac{1}{k} \int_{-\infty}^{\infty} d\xi \int_0^{k_B T_{BG}} \Omega^2 d\Omega \frac{1}{p} [1 - (\frac{k^2 + p^2 - (\Omega/s)^2}{2kp})^2]^{-1/2} \\ & \times [\delta(\xi - \epsilon - \Omega)(n_B(\Omega) + n_F(\xi)) + \delta(\xi - \epsilon + \Omega)(n_B(\Omega) + 1 - n_F(\xi))], \end{aligned} \quad (29)$$

$$\begin{aligned} b(\epsilon, k) = & \frac{\epsilon}{4\pi} \frac{g_D^2}{\rho v^2 s^4} \frac{1}{k^2} \int_{-\infty}^{\infty} d\xi \int_0^{k_B T_{BG}} \Omega^2 d\Omega \frac{k^2 + p^2 - (\Omega/s)^2}{2kp} [1 - (\frac{k^2 + p^2 - (\Omega/s)^2}{2kp})^2]^{-1/2} \\ & \times [\delta(\xi - \epsilon - \Omega)(n_B(\Omega) + n_F(\xi)) + \delta(\xi - \epsilon + \Omega)(n_B(\Omega) + 1 - n_F(\xi))]. \end{aligned} \quad (30)$$

In this work, we are interested in the AH conductivity  $\sigma^I$  which comes from the contribution of electrons on the Fermi surface. For the reason,  $(\epsilon, \mathbf{k})$  is bound to the Fermi surface. The electron energy after scattering with a phonon is  $\xi = \epsilon \pm \omega_q$ . Since  $T_{BG} \ll \epsilon_F$  in our setting, the phonon scattering is quasi-elastic, i.e.,  $\xi \approx \epsilon = \epsilon_F$  in Eq.(28)-(30) and  $a \approx \tilde{a}$ . The self energy can then be written as

$$\Sigma^R(\epsilon, \mathbf{k}) \approx -\frac{i}{2} [a(1 + \frac{\Delta}{\epsilon} \sigma_z) + v \frac{b}{\epsilon} \boldsymbol{\sigma} \cdot \mathbf{k}] \quad (31)$$

as in the main text, where  $a, b$  can be simplified as

$$a(\epsilon, k) = \frac{1}{4\pi} \frac{g_D^2}{\rho v^2 s^3} \frac{\epsilon}{k} \int_0^{k_B T_{BG}} \Omega d\Omega \left(1 - \frac{\Omega^2}{4s^2 k^2}\right)^{-\frac{1}{2}} [2n_B(\Omega) + 1 + n_F(\epsilon + \Omega) - n_F(\epsilon - \Omega)], \quad (32)$$

$$b(\epsilon, k) = \frac{1}{4\pi} \frac{g_D^2}{\rho v^2 s^3} \frac{\epsilon}{k} \int_0^{k_B T_{BG}} \Omega d\Omega \left(1 - \frac{\Omega^2}{2s^2 k^2}\right) \left(1 - \frac{\Omega^2}{4s^2 k^2}\right)^{-\frac{1}{2}} [2n_B(\Omega) + 1 + n_F(\epsilon + \Omega) - n_F(\epsilon - \Omega)]. \quad (33)$$

At the end of the calculation of  $\sigma^I$ , we set  $k = k_F, \epsilon = \epsilon_k = \epsilon_F$ . At  $T \ll T_{BG}$  and  $T \gg T_{BG}$ , we can expand the integrand in Eq.(32) and (33) and get the analytic results of  $a$  and  $b$  in the two limits as shown in Table I in the main text.

## B. Electron Green's function in the first Born approximation

The electron GF in the first Born approximation is

$$\begin{aligned} G^R(\epsilon, \mathbf{k}) &= [G_0^{-1}(\epsilon, \mathbf{k}) - \Sigma^R(\epsilon, \mathbf{k})]^{-1} \\ &= \begin{pmatrix} \epsilon - \Delta + \frac{i}{2}a(1 + \frac{\Delta}{\epsilon}) & -v(k_x - ik_y)(1 - \frac{i}{2}\frac{b}{\epsilon}) \\ -v(k_x + ik_y)(1 - \frac{i}{2}\frac{b}{\epsilon}) & \epsilon + \Delta + \frac{i}{2}a(1 - \frac{\Delta}{\epsilon}) \end{pmatrix}^{-1} \\ &= \frac{1}{\epsilon - \epsilon_k^+ + \frac{i}{2\tau_k^+}} \frac{1}{\epsilon - \epsilon_k^- + \frac{i}{2\tau_k^-}} \left[ (1 + \frac{i}{2\epsilon}a)\epsilon + (1 - \frac{i}{2\epsilon}a)\Delta\sigma_z + (1 - \frac{i}{2\epsilon}b)v\mathbf{k} \cdot \boldsymbol{\sigma} \right], \end{aligned} \quad (34)$$

where  $\epsilon_k^\pm$  are the two energy bands of  $\mathcal{H}_0$  and

$$1/\tau_k^\pm = a \pm \frac{v^2 k^2 b + \Delta^2 a}{\epsilon \epsilon_k}. \quad (35)$$

The above GF can be written in the band basis as

$$G^R(\epsilon, \mathbf{k}) = \frac{|\mathbf{k}, +\rangle \langle \mathbf{k}, +|}{\epsilon - \epsilon_k^+ + \frac{i}{2\tau_k^+}} + \frac{|\mathbf{k}, -\rangle \langle \mathbf{k}, -|}{\epsilon - \epsilon_k^- + \frac{i}{2\tau_k^-}}, \quad (36)$$

where  $|\mathbf{k}, \pm\rangle$  are the two eigenvectors of  $\mathcal{H}_0$ .



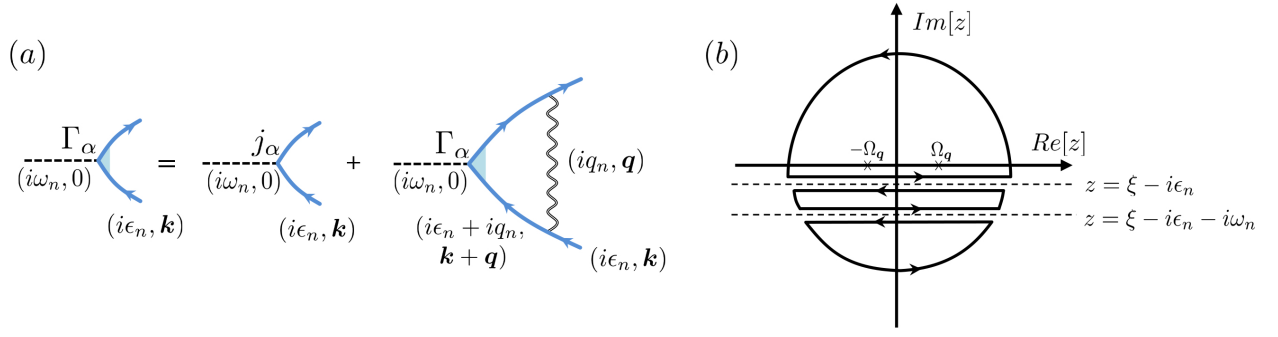


FIG. 4: (a) Feynman diagram of the recursion equation of the renormalized current vertex. The solid and curly lines represent the electron and phonon propagators respectively. (b) The integration contour for the summation of the phonon Matsubara frequency in the recursion equation of the renormalized current vertex.

## II. VERTEX CORRECTION

### A. Recursion equation of the renormalized current vertex

The renormalized current vertex is shown in Fig.4a in the SM and satisfies the recursion equation

$$\hat{\Gamma}_\alpha(i\epsilon_n + i\omega_n, i\epsilon_n; \mathbf{k}) = \hat{j}_\alpha - \frac{1}{\beta} \sum_{iq_n, \mathbf{q}} |g_{\mathbf{q}}|^2 D_0(iq_n, \mathbf{q}) G(i\epsilon'_n + i\omega_n, \mathbf{k}') \hat{\Gamma}_\alpha(i\epsilon'_n + i\omega_n, i\epsilon'_n; \mathbf{k}') G(i\epsilon'_n, \mathbf{k}') \quad (37)$$

where  $i\epsilon'_n \equiv i\epsilon_n + iq_n$ ,  $\mathbf{k}' \equiv \mathbf{k} + \mathbf{q}$ ,  $\hat{j}_\alpha = ev\sigma_\alpha$  is the bare current vertex,  $i\omega_n$  is the external frequency of the vertex and we have set the external momentum of the vertex to be zero.

We may express the current vertex in the Pauli matrix basis as

$$\hat{\Gamma}_\alpha(i\epsilon_n + i\omega_n, i\epsilon_n; \mathbf{k}) = ev\Lambda_{\alpha\beta}(i\epsilon_n + i\omega_n, i\epsilon_n; \mathbf{k})\sigma_\beta, \quad (38)$$

where  $\alpha, \beta = 0, x, y, z$  and the sum over repeated indices is implied in the whole text.

The recursion Eq.(37) then becomes

$$\Lambda_{\alpha\gamma}(i\epsilon_n + i\omega_n, i\epsilon_n; \mathbf{k}) = \delta_{\alpha\gamma} - \frac{1}{\beta} \sum_{iq_n} \sum_{\mathbf{q}} D_0(iq_n, \mathbf{q}) \Lambda_{\alpha\beta}(i\epsilon'_n + i\omega_n, i\epsilon'_n; \mathbf{k} + \mathbf{q}) \mathcal{I}_{\beta\gamma}(i\epsilon'_n + i\omega_n, i\epsilon'_n; \mathbf{k} + \mathbf{q}), \quad (39)$$

where

$$\mathcal{I}_{\beta\gamma}(i\epsilon'_n + i\omega_n, i\epsilon'_n; \mathbf{k} + \mathbf{q}) = \frac{1}{2} \text{Tr}[\sigma_\beta G(iq_n + i\epsilon_n + i\omega_n, \mathbf{k} + \mathbf{q}) \sigma_\gamma G(iq_n + i\epsilon_n, \mathbf{k} + \mathbf{q})] \quad (40)$$

is the polarization operator.

The sum over the Matsubara frequency in Eq.(39) may be done by performing the contour integral in Fig.4b. Denoting

$$Q(i\epsilon_n + i\omega_n, i\epsilon_n) \equiv -\frac{1}{\beta} \sum_{iq_n} D_0(iq_n, \mathbf{q}) \Lambda_{\alpha\beta}(iq_n + i\omega_n + i\epsilon_n, iq_n + i\epsilon_n; \mathbf{k} + \mathbf{q}) \mathcal{I}_{\beta\gamma}(iq_n + i\epsilon_n + i\omega_n, iq_n + i\epsilon_n; \mathbf{k} + \mathbf{q}) \quad (41)$$

and

$$S(i\epsilon_n + i\omega_n, i\epsilon_n) \equiv \int_{\mathcal{C}} \frac{dz}{2\pi i} n_B(z) D_0(z, \mathbf{q}) \Lambda_{\alpha\beta}(z + i\epsilon_n + i\omega_n, z + i\epsilon_n; \mathbf{k} + \mathbf{q}) \mathcal{I}_{\beta\gamma}(z + i\epsilon_n + i\omega_n, z + i\epsilon_n; \mathbf{k} + \mathbf{q}), \quad (42)$$

where  $\mathcal{C}$  is the integration contour in Fig.4b, we get

$$S(i\epsilon_n + i\omega_n, i\epsilon_n) = -Q(i\epsilon_n + i\omega_n, i\epsilon_n) + \sum_{z_j = \pm i\omega_q} \text{Res}[D_0(z = z_j, \mathbf{q})] \Lambda_{\alpha\beta}(z_j + i\epsilon_n + i\omega_n, z_j + i\epsilon_n; \mathbf{k} + \mathbf{q}) \mathcal{I}_{\beta\gamma}(z_j + i\epsilon_n + i\omega_n, z_j + i\epsilon_n; \mathbf{k} + \mathbf{q}) n_B(z_j). \quad (43)$$

The contour integral  $S$  on the circle vanishes and the integral becomes

$$\begin{aligned}
S(i\epsilon_n + i\omega_n, i\epsilon_n) &= \int_{-\infty}^{\infty} \frac{d\xi}{2\pi i} n_B(\xi - i\epsilon_n) D_0(\xi - i\epsilon_n) \\
&\quad [\Lambda_{\alpha\beta}(\xi + i\omega_n, \xi + i0^+) \mathcal{I}_{\beta\gamma}(\xi + i\omega_n, \xi + i0^+) - \Lambda_{\alpha\beta}(\xi + i\omega_n, \xi - i0^+) \mathcal{I}_{\beta\gamma}(\xi + i\omega_n, \xi - i0^+)] \\
&\quad + \int_{-\infty}^{\infty} \frac{d\xi}{2\pi i} n_B(\xi - i\epsilon_n - i\omega_n) D_0(\xi - i\epsilon_n - i\omega_n) \\
&\quad [\Lambda_{\alpha\beta}(\xi + i0^+, \xi - i\omega_n) \mathcal{I}_{\beta\gamma}(\xi + i0^+, \xi - i\omega_n) - \Lambda_{\alpha\beta}(\xi - i0^+, \xi - i\omega_n) \mathcal{I}_{\beta\gamma}(\xi - i0^+, \xi - i\omega_n)]. \quad (44)
\end{aligned}$$

For brevity we have dropped the momentum appeared in Eq.(43) in the above equation.

The dominant vertex correction comes from the  $G^R G^A$  or  $G^A G^R$  term in the polarization operator  $\mathcal{I}$ . For the reason, we perform the analytic continuation  $i\epsilon_n \rightarrow \epsilon - i0^+$ ,  $i\omega_n \rightarrow \omega + i0^+$  and get

$$\begin{aligned}
S^{RA}(\epsilon + \omega, \epsilon) &= S(i\epsilon_n + i\omega_n \rightarrow \epsilon + \omega + i0^+, i\epsilon_n \rightarrow \epsilon - i0^+) \\
&= - \int_{-\infty}^{\infty} \frac{d\xi}{2\pi i} n_F(\xi) D_0^R(\xi - \epsilon) [\Lambda_{\alpha\beta}^{RR}(\xi + \omega, \xi) \mathcal{I}_{\beta\gamma}^{RR}(\xi + \omega, \xi) - \Lambda_{\alpha\beta}^{RA}(\xi + \omega, \xi) \mathcal{I}_{\beta\gamma}^{RA}(\xi + \omega, \xi)] \\
&\quad - \int_{-\infty}^{\infty} \frac{d\xi}{2\pi i} n_F(\xi) D_0^A(\xi - \epsilon - \omega) [\Lambda_{\alpha\beta}^{RA}(\xi, \xi - \omega) \mathcal{I}_{\beta\gamma}^{RA}(\xi, \xi - \omega) - \Lambda_{\alpha\beta}^{AA}(\xi, \xi - \omega) \mathcal{I}_{\beta\gamma}^{AA}(\xi, \xi - \omega)] \\
&\simeq \int_{-\infty}^{\infty} \frac{d\xi}{2\pi i} [n_F(\xi) D_0^R(\xi - \epsilon) \Lambda_{\alpha\beta}^{RA}(\xi + \omega, \xi) \mathcal{I}_{\beta\gamma}^{RA}(\xi + \omega, \xi) - n_F(\xi) D_0^A(\xi - \epsilon - \omega) \Lambda_{\alpha\beta}^{RA}(\xi, \xi - \omega) \mathcal{I}_{\beta\gamma}^{RA}(\xi, \xi - \omega)]. \quad (45)
\end{aligned}$$

In the last equation, we dropped the  $\mathcal{I}^{RR}$  and  $\mathcal{I}^{AA}$  terms because they are small compared to the  $\mathcal{I}^{RA}$  terms.

We are interested in the dc AH conductivity so we take the dc limit  $\omega \rightarrow 0$  at the end and get

$$S^{RA}(\epsilon, \epsilon) = \int_{-\infty}^{\infty} \frac{d\xi}{2\pi i} n_F(\xi) [D_0^R(\xi - \epsilon) - D_0^A(\xi - \epsilon)] \Lambda_{\alpha\beta}^{RA}(\xi, \xi) \mathcal{I}_{\beta\gamma}^{RA}(\xi, \xi). \quad (46)$$

Since

$$D_0^R(\xi - \epsilon) - D_0^A(\xi - \epsilon) = -2i\pi[\delta(\xi - \epsilon - \omega_q) - \delta(\xi - \epsilon + \omega_q)], \quad (47)$$

we get

$$S^{RA}(\epsilon, \epsilon) = - \int_{-\infty}^{\infty} d\xi n_F(\xi) [\delta(\xi - \epsilon - \omega_q) - \delta(\xi - \epsilon + \omega_q)] \Lambda_{\alpha\beta}^{RA}(\xi, \xi) \mathcal{I}_{\beta\gamma}^{RA}(\xi, \xi; \mathbf{k} + \mathbf{q}), \quad (48)$$

where

$$I_{\beta\gamma}^{RA}(\xi, \xi; \mathbf{k} + \mathbf{q}) = \frac{1}{2} \text{Tr}[\sigma_\beta G^R(\xi, \mathbf{k} + \mathbf{q}) \sigma_\gamma G^A(\xi, \mathbf{k} + \mathbf{q})]. \quad (49)$$

Performing the same analytic continuation for the residue terms in Eq.(43) and then taking the limit  $\omega \rightarrow 0$ , we get

$$\begin{aligned}
&\sum_{z_j = \pm\omega_q} \text{Res}[D_0(z = z_j)] \Lambda_{\alpha\beta}(z_j + \epsilon + \omega + i0^+, z_j + \epsilon - i0^+) \mathcal{I}_{\beta\gamma}(z_j + \epsilon + \omega + i0^+, z_j + \epsilon - i0^+) n_B(z_j) \\
&= n_B(\omega_q) \Lambda_{\alpha\beta}^{RA}(\omega_q + \epsilon, \omega_q + \epsilon) \mathcal{I}_{\beta\gamma}^{RA}(\omega_q + \epsilon, \omega_q + \epsilon) - n_B(-\omega_q) \Lambda_{\alpha\beta}^{RA}(-\omega_q + \epsilon, -\omega_q + \epsilon) \mathcal{I}_{\beta\gamma}^{RA}(-\omega_q + \epsilon, -\omega_q + \epsilon) \\
&= \int_{-\infty}^{\infty} d\xi \Lambda_{\alpha\beta}^{RA}(\xi, \xi) \mathcal{I}_{\beta\gamma}^{RA}(\xi, \xi) [\delta(\xi - \epsilon - \omega_q) n_B(\omega_q) + \delta(\xi - \epsilon + \omega_q) (1 + n_B(\omega_q))]. \quad (50)
\end{aligned}$$

From Eq.(43), (48) and (50), we get

$$Q^{RA}(\epsilon, \epsilon) = \int_{-\infty}^{\infty} d\xi \Lambda_{\alpha\beta}^{RA}(\xi, \xi) \mathcal{I}_{\beta\gamma}^{RA}(\xi, \xi) [\delta(\xi - \epsilon - \omega_q) (n_B(\omega_q) + n_F(\xi)) + \delta(\xi - \epsilon + \omega_q) (n_B(\omega_q) + 1 - n_F(\xi))]. \quad (51)$$

The recursion Eq.(39) after analytic continuation to the real axis of the energy becomes

$$\begin{aligned}
\Lambda_{\alpha\gamma}^{RA}(\epsilon, \epsilon; \mathbf{k}) &= \delta_{\alpha\gamma} + \sum_{\mathbf{q}} |g_{\mathbf{q}}|^2 Q^{RA}(\epsilon, \epsilon) \\
&= \delta_{\alpha\gamma} + \sum_{\mathbf{q}} |g_{\mathbf{q}}|^2 \int d\xi \Lambda_{\alpha\beta}^{RA}(\xi, \xi; \mathbf{k} + \mathbf{q}) \mathcal{I}_{\beta\gamma}^{RA}(\xi, \xi; \mathbf{k} + \mathbf{q}) \\
&\quad [\delta(\xi - \epsilon - \omega_{\mathbf{q}})(n_B(\omega_{\mathbf{q}}) + n_F(\xi)) + \delta(\xi - \epsilon + \omega_{\mathbf{q}})(n_B(\omega_{\mathbf{q}}) + 1 - n_F(\xi))].
\end{aligned} \tag{52}$$

The recursion equation of the current vertex  $\Gamma_{\alpha}$  after analytic continuation to real energy axis is then

$$\begin{aligned}
\hat{\Gamma}_{\alpha}^{RA}(\epsilon, \epsilon; \mathbf{k}) &= \hat{j}_{\alpha} + \int d\xi \sum_{\mathbf{q}} |g_{\mathbf{q}}|^2 G^A(\xi, \mathbf{k} + \mathbf{q}) \hat{\Gamma}_{\alpha}^{RA}(\xi, \xi; \mathbf{k} + \mathbf{q}) G^R(\xi, \mathbf{k} + \mathbf{q}) \\
&\quad [\delta(\xi - \epsilon - \omega_{\mathbf{q}})(n_B(\omega_{\mathbf{q}}) + n_F(\xi)) + \delta(\xi - \epsilon + \omega_{\mathbf{q}})(n_B(\omega_{\mathbf{q}}) + 1 - n_F(\xi))].
\end{aligned} \tag{53}$$

To lighten the notation, we drop the superscript  $RA$  in  $\hat{\Gamma}_{\alpha}^{RA}$ ,  $\Lambda_{\alpha\gamma}^{RA}$  and  $\mathcal{I}_{\beta\gamma}^{RA}$  and assume we are discussing the  $RA$  component of these quantities by default in the following text.

## B. Renormalized current vertex in the band basis

The dominant vertex correction comes from the phonon scatterings of electrons within the upper band. It is then convenient to work in the eigenstate band basis (chiral basis) to compute the dominant vertex correction.

The renormalized current vertex in the Feynman diagrams of the AH conductivities corresponds to the band diagonal matrix element

$$\begin{aligned}
\Gamma_{\alpha}^{++}(\epsilon, \epsilon; \mathbf{k}) &\equiv \langle \mathbf{k}, + | \hat{\Gamma}_{\alpha}(\epsilon, \epsilon; \mathbf{k}) | \mathbf{k}, + \rangle \\
&= j_{\alpha}^{++}(\mathbf{k}) + \int d\xi \sum_{\mathbf{q}} |g_{\mathbf{q}}|^2 G^{R+}(\xi, \mathbf{k} + \mathbf{q}) G^{A+}(\xi, \mathbf{k} + \mathbf{q}) \Gamma_{\alpha}^{++}(\xi, \xi; \mathbf{k} + \mathbf{q}) |\langle \mathbf{k} + \mathbf{q}, + | \mathbf{k}, + \rangle|^2 \\
&\quad [\delta(\xi - \epsilon - \omega_{\mathbf{q}})(n_B(\omega_{\mathbf{q}}) + n_F(\xi)) + \delta(\xi - \epsilon + \omega_{\mathbf{q}})(n_B(\omega_{\mathbf{q}}) + 1 - n_F(\xi))],
\end{aligned} \tag{54}$$

where  $j_{\alpha}^{++}(\mathbf{k}) = \langle \mathbf{k}, + | \hat{j}_{\alpha} | \mathbf{k}, + \rangle = ev \frac{vk_{\alpha}}{\epsilon_k}$  and

$$G^{R/A,+}(\epsilon, \mathbf{k}) = \langle \mathbf{k}, + | \hat{G}^{R/A} | \mathbf{k}, + \rangle = \frac{1}{\epsilon - \epsilon_k^+ \pm \frac{i}{2\tau_k^+}}. \tag{55}$$

The recursion Eq.(54) of the current vertex is hard to solve exactly. We then apply the approximation that the scattering by phonon is quasi-elastic as before, i.e.,  $\epsilon_{k'} = \epsilon_k \pm \omega_q \approx \epsilon_k$ ,  $k' \approx k$  in Eq.(54), where  $\mathbf{k}' \equiv \mathbf{k} + \mathbf{q}$ . Under this approximation, we can compute the renormalized current vertex  $\Gamma_{\alpha}^{++}(\epsilon, \epsilon; \mathbf{k})$  order by order by iteration of Eq.(54). In the following, we show this process for  $\Gamma_x^{++}(\epsilon, \epsilon; \mathbf{k})$ .

The sum over the phonon momentum  $\mathbf{q}$  in Eq.(54) may be replaced by the sum over  $\mathbf{k}'$  as in the calculation of the self-energy and Eq.(54) becomes

$$\begin{aligned}
\Gamma_{\alpha}^{++}(\epsilon, \epsilon; \mathbf{k}) &= j_{\alpha}^{++}(\mathbf{k}) + \int d\xi \int \frac{k' dk'}{(2\pi)^2} \int_0^{2\pi} d\theta |g_{\mathbf{q}}|^2 G^{R+}(\xi, \mathbf{k}') G^{A+}(\xi, \mathbf{k}') \Gamma_{\alpha}^{++}(\xi, \xi; \mathbf{k}') |\langle \mathbf{k}', + | \mathbf{k}, + \rangle|^2 \\
&\quad [\delta(\xi - \epsilon - \omega_{\mathbf{q}})(n_B(\omega_{\mathbf{q}}) + n_F(\xi)) + \delta(\xi - \epsilon + \omega_{\mathbf{q}})(n_B(\omega_{\mathbf{q}}) + 1 - n_F(\xi))].
\end{aligned} \tag{56}$$

For  $\Gamma_x^{++}$ , the zeroth order is  $j_x^{++}(\mathbf{k}) = ev^2 k_x / \epsilon_k$ . The first order can be obtained by replacing  $\Gamma_{\alpha}^{++}(\xi, \xi; \mathbf{k}')$  in Eq.(56) with  $j_x^{++}(\mathbf{k}')$ . Since  $v^2 k' dk' = \epsilon_{k'} d\epsilon_{k'}$ , we can replace the integration over  $dk'$  by  $d\epsilon_{k'}$  in Eq.(56). Employing

$$G^{R+}(\xi, \mathbf{k}') G^{A+}(\xi, \mathbf{k}') = 2\pi \tau_{k'}^+ \delta(\xi - \epsilon_{k'}), \quad \tau_{k'}^+ = 1/[a + \frac{bv^2 k'^2 + a\Delta^2}{\xi \epsilon_{k'}}], \tag{57}$$

$$|\langle \mathbf{k}', + | \mathbf{k}, + \rangle|^2 = \frac{1}{2}(1 + \cos \alpha' \cos \alpha + \sin \alpha' \sin \alpha \cos \theta), \tag{58}$$

$$j_x^{++}(\mathbf{k}') = ev \frac{vk'}{\epsilon_{k'}} \cos(\theta + \theta_0), \tag{59}$$

we get the first order of  $\Gamma_x^{++}$  after integration over  $dk'$  as

$$\Gamma_x^{(1),++}(\epsilon, \epsilon; \mathbf{k}) \approx g_D^2 \frac{\hbar}{4\pi\rho s^2 v^2} \frac{ev^2 k}{\epsilon_k} \tau_k^+ \int_{-\infty}^{\infty} \xi d\xi \int_0^{2\pi} d\theta \int_0^{2k_B T_{BG}} \Omega d\Omega \delta(\Omega - \omega_q) (\cos \theta_0 \cos \theta - \sin \theta_0 \sin \theta) \frac{1}{2} (1 + \cos^2 \alpha + \sin^2 \alpha \cos \theta) [\delta(\xi - \epsilon - \Omega)(n_B(\Omega) + n_F(\xi)) + \delta(\xi - \epsilon + \Omega)(n_B(\Omega) + 1 - n_F(\xi))]. \quad (60)$$

In the above integration, we have applied the quasi-elastic scattering approximation so that  $\tau_{k'}^+ \approx \tau_k^+$ ,  $\cos \alpha' \approx \cos \alpha = \Delta/\epsilon_k$ ,  $\sin \alpha' \approx \sin \alpha$ . We also introduced an integration over  $d\Omega$  through the factor  $\delta(\Omega - \omega_q)$  to convert the integration over the angle  $d\theta$  to the integration over  $d\Omega$  as in the calculation of the self-energy. The integration over  $d\theta$  can be done using the following integrals

$$\int_0^{2\pi} d\theta \delta(\Omega - \omega_q) \approx \frac{2}{sk} \frac{1}{|\cos \frac{\theta_\Omega}{2}|} \approx \frac{2}{sk} \frac{1}{\sqrt{1 - \frac{\Omega^2}{4s^2 k^2}}}, \quad \theta_\Omega \equiv 2 \arcsin \frac{\Omega}{2sk}, \quad (61)$$

$$\int_0^{2\pi} d\theta \cos \theta \delta(\Omega - \omega_q) \approx \frac{2}{sk} \frac{\cos \theta_\Omega}{|\cos \frac{\theta_\Omega}{2}|} \approx \frac{2}{sk} \frac{1 - \Omega^2/2s^2 k^2}{\sqrt{1 - \frac{\Omega^2}{4s^2 k^2}}}, \quad (62)$$

$$\int_0^{2\pi} d\theta \cos^2 \theta \delta(\Omega - \omega_q) \approx \frac{2}{sk} \frac{\cos^2 \theta_\Omega}{|\cos \frac{\theta_\Omega}{2}|} \approx \frac{2}{sk} \frac{(1 - \Omega^2/2s^2 k^2)^2}{\sqrt{1 - \frac{\Omega^2}{4s^2 k^2}}}, \quad (63)$$

$$\int_0^{2\pi} \sin \theta d\theta \delta(\Omega - \omega_q) = 0, \quad \int_0^{2\pi} \sin \theta \cos \theta d\theta \delta(\Omega - \omega_q) = 0. \quad (64)$$

After the integration over  $d\theta$  in Eq.(60), we get the first order of  $\Gamma_x^{++}$  as

$$\begin{aligned} \Gamma_x^{(1),++}(\epsilon, \epsilon; \mathbf{k}) &\approx \frac{g_D^2}{4\pi\rho s^4 v^2 k^2} \frac{ev^2 k_x}{\epsilon_k} \tau_k^+ \int_0^{2k_B T_{BG}} d\Omega \Omega^2 \int_{-\infty}^{\infty} \xi d\xi \frac{\cos \theta_\Omega}{|\sin \theta_\Omega|} \times [(1 + \frac{\Delta^2}{\xi \epsilon_k}) + \frac{v^2 k^2}{\xi \epsilon_k} \cos \theta_\Omega] \\ &\times [\delta(\xi - \epsilon - \Omega)(n_B(\Omega) + n_F(\xi)) + \delta(\xi - \epsilon + \Omega)(n_B(\Omega) + 1 - n_F(\xi))] \\ &\approx \frac{ev^2 k_x}{\epsilon_k} \tau_k^+ [(1 + \frac{\Delta^2}{\epsilon \epsilon_k}) b(\epsilon, k) + \frac{v^2 k^2}{\epsilon \epsilon_k} c(\epsilon, k)], \end{aligned} \quad (65)$$

where  $b(\epsilon, k)$  is defined in Eq.(30) and  $c(\epsilon, k)$  is defined as

$$\begin{aligned} c(\epsilon, k) &= \frac{1}{4\pi} \frac{g_D^2}{\rho s^4 v^2} \frac{1}{k^2} \int_{-\infty}^{\infty} \xi d\xi \int_0^{k_B T_{BG}} d\Omega \Omega^2 \frac{\cos^2 \theta_\Omega}{|\sin \theta_\Omega|} \\ &\times [\delta(\xi - \epsilon - \Omega)(n_B(\Omega) + n_F(\xi)) + \delta(\xi - \epsilon + \Omega)(n_B(\Omega) + 1 - n_F(\xi))] \\ &\approx \frac{1}{4\pi} \frac{g_D^2 \hbar}{\rho s^3 v^2} \frac{\epsilon}{k} \int_0^{k_B T_{BG}} \Omega d\Omega (1 - \frac{\Omega^2}{2s^2 k^2})^2 (1 - \frac{\Omega^2}{4s^2 k^2})^{-\frac{1}{2}} [2n_B(\Omega) + 1 + n_F(\epsilon + \Omega) - n_F(\epsilon - \Omega)]. \end{aligned} \quad (66)$$

We denote

$$\lambda(\epsilon, k) = \tau_k^+ [(1 + \frac{\Delta^2}{\epsilon \epsilon_k}) b(\epsilon, k) + \frac{v^2 k^2}{\epsilon \epsilon_k} c(\epsilon, k)]. \quad (67)$$

From Eq.(65), we get

$$\Gamma_x^{(1),++}(\epsilon, \epsilon; \mathbf{k}) = \lambda(\epsilon, k) j_x^{++}(\mathbf{k}). \quad (68)$$

By iteration order by order we get

$$\Gamma_x^{(n),++}(\epsilon, \epsilon; \mathbf{k}) = \lambda^n(\epsilon, k) j_x^{++}(\mathbf{k}), \quad (69)$$

and the renormalized current vertex

$$\Gamma_x^{++} = \sum_{n=0}^{\infty} \Gamma_x^{(n),++}(\epsilon, \epsilon; \mathbf{k}) = \frac{1}{1 - \lambda} j_x^{++}(\mathbf{k}). \quad (70)$$

Since the system is isotropic,  $\Gamma_y^{++} = \sum_{n=0}^{\infty} \Gamma_y^{(n),++}(\epsilon, \epsilon; \mathbf{k}) = \frac{1}{1-\lambda} j_y^{++}(\mathbf{k})$ .

We have checked that the current vertex renormalization factor  $\gamma \equiv \frac{1}{1-\lambda}$  is equal to  $\tilde{\tau}_k^{tr}/\tau_k^+$  where  $\tilde{\tau}_k^{tr}$  and  $\tau_k^+$  are respectively the transport and mean lifetime of the upper band electrons with phonon scatterings defined in Ref. [19] as

$$1/\tau_k^+ = \sum_{\mathbf{k}'} \omega_{\mathbf{k}',\mathbf{k}} \frac{1 - f_{\mathbf{k}'}^0}{1 - f_{\mathbf{k}}^0}, \quad (71)$$

$$1/\tilde{\tau}_k^{tr} = \sum_{\mathbf{k}'} \omega_{\mathbf{k}',\mathbf{k}} \frac{1 - f_{\mathbf{k}'}^0}{1 - f_{\mathbf{k}}^0} (1 - \cos \phi_{\mathbf{k}',\mathbf{k}}), \quad (72)$$

where  $\omega_{\mathbf{k}',\mathbf{k}}$  is the scattering rate from  $\mathbf{k}$  to  $\mathbf{k}'$ ,  $\phi_{\mathbf{k}',\mathbf{k}}$  is the angle between  $\mathbf{k}$  and  $\mathbf{k}'$  and  $f_{\mathbf{k}}^0$  is the Fermi distribution function for energy  $\epsilon_k$ . Note that  $1/\tau_k^+$  defined in Eq.(71) is also equal to that in Eq.(35).

### III. ANOMALOUS HALL CONDUCTIVITY

The extrinsic contribution of the dc AH conductivity comes from  $\sigma_{xy}^I$  which can be written as

$$\sigma_{xy}^I = e^2 v^2 \sum_{\mathbf{k}} \int \frac{d\epsilon}{2\pi} (-\partial_{\epsilon} n_F(\epsilon)) \text{Tr}[\hat{\Gamma}_x(\epsilon, \epsilon, \mathbf{k}) G^R(\epsilon, \mathbf{k}) \sigma_y G^A(\epsilon, \mathbf{k})]. \quad (73)$$

Since  $\partial_{\epsilon} n_F(\epsilon) \sim \delta(\epsilon - \epsilon_F)$ , the contribution to  $\sigma_{xy}^I$  comes from the electrons on the Fermi surface.

The contribution to  $\sigma_{xy}^I$  can be separated to three parts due to different mechanisms: the intrinsic, the side jump and the skew scattering contributions. The intrinsic contribution is due to the non-trivial band structure of the clean system and has been calculated in previous works for 2D massive Dirac metals [10]. The side jump and skew scattering contributions can be most easily separated by expanding the trace in Eq.(73) in the chiral basis, as shown in our previous work [23]. The resulting side jump and skew scattering conductivities are depicted by the Feynman diagrams in the chiral basis in Fig.1 of the main text or Fig.5 and Fig.6 in the SM.

#### A. Side jump contribution

We first calculate the side jump contribution. The dc AH conductivity from Fig.5a and b can be written as

$$\sigma_{xy}^{a+b} = \sum_{\mathbf{k}} \int \frac{d\epsilon}{2\pi} (-\partial_{\epsilon} n_F(\epsilon)) [\Gamma_x'^{+-}(\epsilon, \epsilon; \mathbf{k}) G_0^{R-}(\epsilon, \mathbf{k}) j_y^{-+}(\mathbf{k}) G_0^{A+}(\epsilon, \mathbf{k}) + \Gamma_x'^{-+}(\epsilon, \epsilon; \mathbf{k}) G_0^{R+}(\epsilon, \mathbf{k}) j_y^{+-}(\mathbf{k}) G_0^{A-}(\epsilon, \mathbf{k})], \quad (74)$$

where  $\hat{\Gamma}_x' \equiv \hat{\Gamma}_x - \hat{j}_x$  and  $\Gamma_x'^{+-} \equiv \langle \mathbf{k}, + | \hat{\Gamma}_x' | \mathbf{k}, - \rangle$ .

Applying the recursion Eq.(53) of the renormalized current vertex  $\hat{\Gamma}_x$ , we get

$$\begin{aligned} \Gamma_x'^{+-}(\epsilon, \epsilon; \mathbf{k}) &= \int d\xi \sum_{\mathbf{k}'} |g_{\mathbf{k}'-\mathbf{k}}|^2 G^{R+}(\xi, \mathbf{k}') G^{A+}(\xi, \mathbf{k}') \Gamma_x^{++}(\xi, \xi; \mathbf{k}') \langle \mathbf{k}, + | \mathbf{k}', + \rangle \langle \mathbf{k}', + | \mathbf{k}, - \rangle \\ &\times [\delta(\xi - \epsilon - \omega_{\mathbf{k}'-\mathbf{k}})(n_B(\omega_{\mathbf{k}'-\mathbf{k}}) + n_F(\xi)) + \delta(\xi - \epsilon + \omega_{\mathbf{k}-\mathbf{k}'})(n_B(\omega_{\mathbf{k}-\mathbf{k}'} + 1 - n_F(\xi))], \end{aligned} \quad (75)$$

where

$$\langle \mathbf{k}, + | \mathbf{k}', + \rangle = \cos \frac{\alpha'}{2} \cos \frac{\alpha}{2} + \sin \frac{\alpha'}{2} \sin \frac{\alpha}{2} e^{i\theta}, \quad \langle \mathbf{k}', + | \mathbf{k}, - \rangle = \cos \frac{\alpha'}{2} \sin \frac{\alpha}{2} - \sin \frac{\alpha'}{2} \cos \frac{\alpha}{2} e^{-i\theta}, \quad (76)$$

$$G^{R+}(\xi, \mathbf{k}') G^{A+}(\xi, \mathbf{k}') = 2\pi \tau_k^+ \delta(\xi - \epsilon_{k'}), \quad \text{and} \quad \Gamma_x^{++}(\epsilon, \epsilon; \mathbf{k}) = \frac{1}{1-\lambda} \frac{ev^2 k_x}{\epsilon}. \quad (77)$$

The sum over  $\mathbf{k}'$  in Eq.(75) can be done by the same procedure as for the calculation of  $\Gamma_x^{(1),++}$  under the quasi-elastic scattering approximation. We get

$$\Gamma_x'^{+-}(\epsilon, \epsilon; \mathbf{k}) = \frac{\tau_k^+}{1-\lambda(\epsilon)} \frac{v^2 k}{\epsilon^2} \left[ \frac{\Delta}{\epsilon_k} (b(\epsilon, k) - c(\epsilon, k)) k_x - id(\epsilon, k) k_y \right], \quad (78)$$

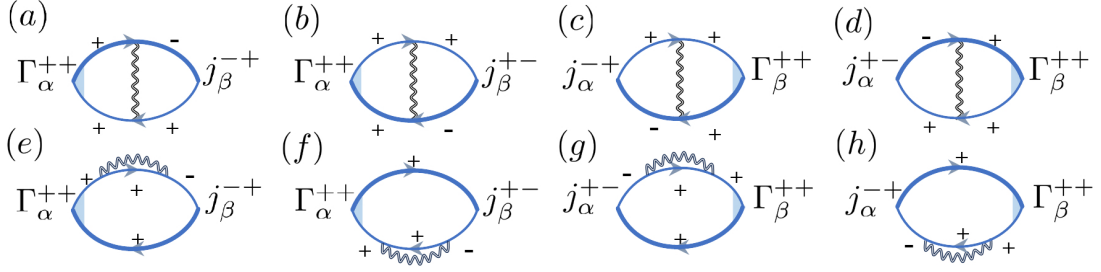


FIG. 5: (a) Feynman diagrams of the side jump conductivity in the chiral basis. The thin and thick solid lines represent the bare electron GF and the electron GF in the first Born approximation respectively. The curvy lines represent the phonon propagators. Note that replacing the thin solid lines by the thick ones in the diagrams, as shown in Fig.1 of the main text, does not change the AH conductivity of the diagrams.

where  $d(\epsilon, k) = a(\epsilon, k) - c(\epsilon, k)$ . Similarly, we get

$$\Gamma_y'^{-}(\epsilon, \epsilon; \mathbf{k}) = \frac{\tau_k^+}{1 - \lambda(\epsilon)} \frac{v^2 k}{\epsilon^2} \left[ \frac{\Delta}{\epsilon_k} (b(\epsilon, k) - c(\epsilon, k)) k_y + i d(\epsilon, k) k_x \right]. \quad (79)$$

With the above ingredients, we can compute the AH conductivity in Eq.(74) corresponding to the Feynman diagrams in Fig.5(a) and (b):

$$\sigma_{xy}^{a+b} = \frac{1}{2\pi} \sum_{\mathbf{k}} [\Gamma_x'^{-}(\epsilon, \epsilon; \mathbf{k}) G_0^{R-}(\epsilon, \mathbf{k}) j_y^{-+}(\mathbf{k}) G_0^{A+}(\epsilon, \mathbf{k}) + \Gamma_x'^{-}(\epsilon, \epsilon; \mathbf{k}) G_0^{R+}(\epsilon, \mathbf{k}) j_y^{+-}(\mathbf{k}) G_0^{A-}(\epsilon, \mathbf{k})] |_{\epsilon=\epsilon_F}, \quad (80)$$

where

$$j_y^{-+}(\mathbf{k}) = ev \sigma_y^{-+}(\mathbf{k}), \quad \sigma_y^{-+}(\mathbf{k}) = -i \cos \theta_0 - \cos \alpha \sin \theta_0, \quad (81)$$

$$G_0^{R-}(\epsilon, k) = \frac{1}{\epsilon - \epsilon_k^- + i\eta}, \quad G_0^{A+}(\epsilon, k) = \frac{1}{\epsilon - \epsilon_k^+ - i\eta}, \quad \eta \rightarrow 0^+, \quad (82)$$

$$\Gamma_x'^{-} j_y^{-+} = [\Gamma_x'^{-} j_y^{+-}]^* = e^2 v^2 \frac{i \tau_k^+}{1 - \lambda(\epsilon)} \frac{v^2 k^2}{\epsilon^2} [- (b(\epsilon, k) - c(\epsilon, k)) \cos \alpha \cos^2 \theta_0 + d(\epsilon, k) \cos \alpha \sin^2 \theta_0]. \quad (83)$$

The sum over  $\mathbf{k}$  in Eq.(80) may be converted to the integral

$$\sum_{\mathbf{k}} \rightarrow \int_0^{+\infty} \frac{k dk}{(2\pi)^2} \int_0^{2\pi} d\theta_0. \quad (84)$$

After the integration over  $d\theta_0$ , we get

$$\begin{aligned} \sigma_{xy}^{a+b} &= \frac{i}{2} \frac{\Delta}{\epsilon^2} \int \frac{k dk}{4\pi^2} \frac{\tau_k^+}{1 - \lambda(\epsilon)} \frac{e^2 v^4 k^2}{\epsilon_k} [a(\epsilon, k) - b(\epsilon, k)] \left( \frac{1}{\epsilon - \epsilon_k^- + i\eta} \frac{1}{\epsilon - \epsilon_k^+ - i\eta} - \frac{1}{\epsilon - \epsilon_k^+ + i\eta} \frac{1}{\epsilon - \epsilon_k^- - i\eta} \right) |_{\epsilon=\epsilon_F} \\ &= \frac{i}{8\pi^2} \frac{\Delta}{\epsilon^2} \int k dk \frac{\tau_k^+}{1 - \lambda(\epsilon)} \frac{e^2 v^4 k^2}{\epsilon_k} [a(\epsilon, k) - b(\epsilon, k)] \frac{1}{\epsilon + \epsilon_k^+} \times 2i\pi \delta(\epsilon - \epsilon_k^+) |_{\epsilon=\epsilon_F} \\ &= -\frac{e^2}{8\pi} \frac{\Delta}{\epsilon_F} \left( 1 - \frac{\Delta^2}{\epsilon_F^2} \right) \frac{\tau_{k_F}^+}{1 - \lambda(\epsilon_F, k_F)} [a(\epsilon_F, k_F) - b(\epsilon_F, k_F)]. \end{aligned} \quad (85)$$

The total contribution from the diagrams Fig.5(c) and (d) is identical to that of Fig.5(a) and (b). We then get the total side jump contribution due to Fig.5 (a)-(d) as

$$\sigma_{xy}^{side, (1)} = -\frac{e^2}{4\pi} \frac{\Delta}{\epsilon_F} \left( 1 - \frac{\Delta^2}{\epsilon_F^2} \right) \frac{\tau_{k_F}^+}{1 - \lambda(\epsilon_F, k_F)} [a(\epsilon_F, k_F) - b(\epsilon_F, k_F)]. \quad (86)$$

We next compute the contribution from Fig.5(e). The AH conductivity corresponding to this diagram can be written as

$$\sigma_{xy}^e = \frac{1}{2\pi} \sum_{\mathbf{k}} \Gamma_x^{++} G_0^{R+} \Sigma^{R,+-} G_0^{R-} j_y^{-+} G^{A+} |_{\epsilon=\epsilon_F}, \quad (87)$$

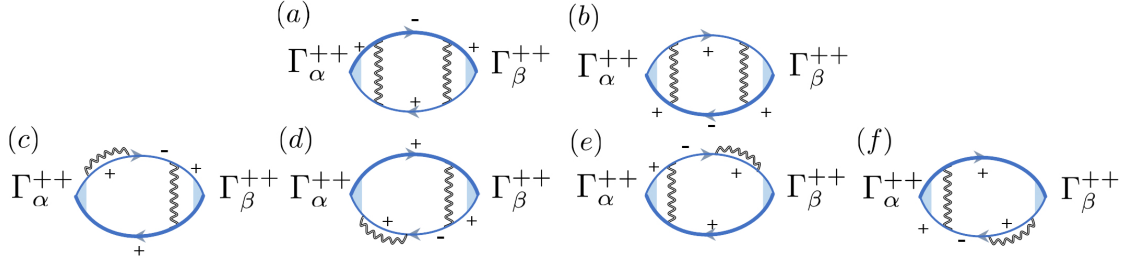


FIG. 6: Feynman diagrams of the skew scattering conductivity in the chiral basis. The notations are the same as in Fig.5.

where

$$\Sigma^{R,+ -} = \langle + | \Sigma^R | - \rangle = -\frac{i}{2} \frac{vk\Delta}{\epsilon\epsilon_k} (a - b). \quad (88)$$

After the sum over  $\mathbf{k}$  in Eq.(87), we get

$$\sigma_{xy}^e = -\frac{e^2}{16\pi\epsilon_F} \left(1 - \frac{\Delta^2}{\epsilon_F^2}\right) \frac{\tau_{k_F}^+}{1 - \lambda(\epsilon_F, k_F)} (a(\epsilon_F, k_F) - b(\epsilon_F, k_F)). \quad (89)$$

Each of the diagrams (f)-(h) contributes the same as diagram (e) in Fig.5 so the total contribution from the diagrams (e)-(h) is

$$\sigma_{xy}^{side,(2)} = -\frac{e^2}{4\pi\epsilon_F} \left(1 - \frac{\Delta^2}{\epsilon_F^2}\right) \frac{\tau_{k_F}^+}{1 - \lambda(\epsilon_F, k_F)} (a(\epsilon_F, k_F) - b(\epsilon_F, k_F)). \quad (90)$$

The total side jump conductivity is

$$\begin{aligned} \sigma_{xy}^{side} &= \sigma_{xy}^{side,(1)} + \sigma_{xy}^{side,(2)} \\ &= -\frac{e^2}{2\pi\epsilon_F} \left(1 - \frac{\Delta^2}{\epsilon_F^2}\right) \frac{\tau_{k_F}^+}{1 - \lambda(\epsilon_F, k_F)} (a(\epsilon_F, k_F) - b(\epsilon_F, k_F)) \\ &= -\frac{e^2}{2\pi\epsilon_F} \left(1 - \frac{\Delta^2}{\epsilon_F^2}\right) \frac{a(\epsilon_F, k_F) - b(\epsilon_F, k_F)}{a(\epsilon_F, k_F) - c(\epsilon_F, k_F) + \frac{\Delta^2}{\epsilon_F^2} [a(\epsilon_F, k_F) + c(\epsilon_F, k_F) - 2b(\epsilon_F, k_F)]}. \end{aligned} \quad (91)$$

## B. Skew scattering contribution

The skew scattering contribution is described by the Feynman diagrams in Fig.6. The AH conductivity due to diagrams (a) and (b) in Fig.6 can be written as

$$\sigma_{xy}^{sk,a+b} = \sum_{\mathbf{k}} \int \frac{d\epsilon}{2\pi} (-\partial_{\epsilon} n_F(\epsilon)) [\Gamma_x'^{+-} G^{R-} \Gamma_y'^{-+} G_0^{A+} + \Gamma_x'^{-+} G_0^{R+} \Gamma_y'^{+-} G^{A-}], \quad (92)$$

where  $\Gamma_x'^{+-} = [\Gamma_x'^{-+}]^*$ ,  $\Gamma_y'^{+-} = [\Gamma_y'^{-+}]^*$  and  $\Gamma_x'^{+-}, \Gamma_y'^{+-}$  are given in Eq.(78) and (79). And  $G_0$  and  $G$  are the bare electron GF and the GF in the first Born approximation respectively, both of which are given in the previous text. After the sum over  $\mathbf{k}$ , we get

$$\sigma_{xy}^{sk,a+b} = \frac{e^2\Delta}{4\pi\epsilon_F} \left(1 - \frac{\Delta^2}{\epsilon_F^2}\right)^2 \left[ \frac{\tau_{k_F}^+}{1 - \lambda(\epsilon_F, k_F)} \right]^2 [b(\epsilon_F, k_F) - c(\epsilon_F, k_F)] d(\epsilon_F, k_F). \quad (93)$$

The AH conductivity due to diagram (c) in Fig.6 can be written as

$$\begin{aligned} \sigma_{xy}^{sk,c} &= \int \frac{d\epsilon}{2\pi} (-\partial_{\epsilon} n_F(\epsilon)) \sum_{\mathbf{k}} \Gamma_x^{++} G_0^{R+} \Sigma^{R,+ -} G_0^{R-} \Gamma_y'^{-+} G^{A+} \\ &= -\frac{e^2\Delta}{16\pi\epsilon_F} \left(1 - \frac{\Delta^2}{\epsilon_F^2}\right)^2 \left[ \frac{\tau_{k_F}^+}{1 - \lambda(\epsilon_F, k_F)} \right]^2 [a(\epsilon_F, k_F) - b(\epsilon_F, k_F)] d(\epsilon_F, k_F) \end{aligned} \quad (94)$$

The contribution from each diagram of Fig.6(e)-(f) is identical to that of (c). The total skew scattering contribution of Fig.6(a)-(f) is then

$$\sigma_{xy}^{sk-nc} = -\frac{e^2 \Delta}{4\pi \epsilon_F} \left(1 - \frac{\Delta^2}{\epsilon_F^2}\right)^2 \left[ \frac{\tau_{k_F}^+}{1 - \lambda(\epsilon_F, k_F)} \right]^2 [a(\epsilon_F, k_F) + c(\epsilon_F, k_F) - 2b(\epsilon_F, k_F)] d(\epsilon_F, k_F) \quad (95)$$

where  $\frac{\tau_{k_F}^+}{1 - \lambda(\epsilon_F, k_F)} = \{a(\epsilon_F, k_F) - c(\epsilon_F, k_F) + \frac{\Delta^2}{\epsilon_F^2} [a(\epsilon_F, k_F) + c(\epsilon_F, k_F) - 2b(\epsilon_F, k_F)]\}^{-1}$  and  $d(\epsilon_F, k_F) = a(\epsilon_F, k_F) - c(\epsilon_F, k_F)$ .

### C. Scaling function of the AH conductivity

From Eq.(91) and (95), the side jump and skew scattering conductivities are expressed by three parameters  $a(\epsilon_F, k_F)$ ,  $b(\epsilon_F, k_F)$ ,  $c(\epsilon_F, k_F)$ , whose full expressions are shown in Eq.(28), (30) and (66) and their analytical results at  $T \ll T_{BG}$  and  $T \gg T_{BG}$  are shown in Table I in the main text.

If we define a rescaled temperature  $t \equiv T/T_{BG}$ , the parameters  $a(\epsilon_F, k_F)$ ,  $b(\epsilon_F, k_F)$ ,  $c(\epsilon_F, k_F)$  can be written as

$$a(\epsilon_F, k_F) = C\tilde{a}(t); \quad b(\epsilon_F, k_F) = C\tilde{b}(t); \quad c(\epsilon_F, k_F) = C\tilde{c}(t), \quad (96)$$

where

$$C \equiv \frac{1}{2\pi} \frac{g_D^2}{\rho v^2 s^3} \frac{\epsilon_F}{k_F} (k_B T)^2 \quad (97)$$

and

$$\tilde{a}(t) = \int_0^{1/t} dx (1 - t^2 x^2)^{-\frac{1}{2}} \left( \frac{1}{e^x - 1} + \frac{1}{e^x + 1} \right), \quad (98)$$

$$\tilde{b}(t) = \int_0^{1/t} dx (1 - 2t^2 x^2)(1 - t^2 x^2)^{-\frac{1}{2}} \left( \frac{1}{e^x - 1} + \frac{1}{e^x + 1} \right), \quad (99)$$

$$\tilde{c}(t) = \int_0^{1/t} dx (1 - 2t^2 x^2)^2 (1 - t^2 x^2)^{-\frac{1}{2}} \left( \frac{1}{e^x - 1} + \frac{1}{e^x + 1} \right). \quad (100)$$

The side jump and skew scattering conductivities can then be expressed in terms of  $\tilde{a}(t)$ ,  $\tilde{b}(t)$  and  $\tilde{c}(t)$  as

$$\sigma_{xy}^{side} \left( \frac{\Delta}{\epsilon_F}, t \right) = -\frac{e^2}{2\pi} \frac{\Delta}{\epsilon_F} \left( 1 - \frac{\Delta^2}{\epsilon_F^2} \right) \frac{[\tilde{a}(t) - \tilde{b}(t)]}{\tilde{a}(t) - \tilde{c}(t) + \frac{\Delta^2}{\epsilon_F^2} [\tilde{a}(t) + \tilde{c}(t) - 2\tilde{b}(t)]}, \quad (101)$$

$$\sigma_{xy}^{sk-nc} \left( \frac{\Delta}{\epsilon_F}, t \right) = -\frac{e^2 \Delta}{4\pi \epsilon_F} \left( 1 - \frac{\Delta^2}{\epsilon_F^2} \right)^2 \frac{[\tilde{a}(t) + \tilde{c}(t) - 2\tilde{b}(t)][\tilde{a}(t) - \tilde{c}(t)]}{\left\{ \tilde{a}(t) - \tilde{c}(t) + \frac{\Delta^2}{\epsilon_F^2} [\tilde{a}(t) + \tilde{c}(t) - 2\tilde{b}(t)] \right\}^2}, \quad (102)$$

which depend only on  $\Delta/\epsilon_F$  and  $t \equiv T/T_{BG}$ . The expansions of  $\tilde{a}$ ,  $\tilde{b}$ ,  $\tilde{c}$  and  $\sigma_{xy}^{side}$ ,  $\sigma_{xy}^{sk-nc}$  in Eq.(98)-(102) in the limit  $T \ll T_{BG}$  and  $T \gg T_{BG}$  are shown in Table I in the main text.

## IV. SCREENING EFFECT

We discuss the screening effect due to e-e interaction in this section. To take into account this effects, we add the Thomas-Fermi (TF) screening factor to the deformation potential, i.e., we replace  $g_D$  by  $g_D \frac{q}{q + q_{TF}}$  where  $q_{TF} = \alpha \epsilon_F / v$  is the TF wave-vector for 2D massive Dirac metals and  $\alpha = e^2 / \hbar v$  is the fine structure constant. With this replacement,



the only change we need to make in the calculation is for  $\tilde{a}(t), \tilde{b}(t), \tilde{c}(t)$  which are now

$$\tilde{a}^{sc}(t) = \int_0^{1/t} x dx \left( \frac{x}{x + \frac{\alpha}{2t} \frac{1}{\sqrt{1-\Delta^2/\epsilon_F^2}}} \right)^2 (1-t^2x^2)^{-\frac{1}{2}} \left( \frac{1}{e^x-1} + \frac{1}{e^x+1} \right), \quad (103)$$

$$\tilde{b}^{sc}(t) = \int_0^{1/t} x dx \left( \frac{x}{x + \frac{\alpha}{2t} \frac{1}{\sqrt{1-\Delta^2/\epsilon_F^2}}} \right)^2 (1-2t^2x^2)(1-t^2x^2)^{-\frac{1}{2}} \left( \frac{1}{e^x-1} + \frac{1}{e^x+1} \right), \quad (104)$$

$$\tilde{c}^{sc}(t) = \int_0^{1/t} x dx \left( \frac{x}{x + \frac{\alpha}{2t} \frac{1}{\sqrt{1-\Delta^2/\epsilon_F^2}}} \right)^2 (1-2t^2x^2)^2(1-t^2x^2)^{-\frac{1}{2}} \left( \frac{1}{e^x-1} + \frac{1}{e^x+1} \right). \quad (105)$$

From the above equations, we can see that  $\tilde{a}^{sc}(t), \tilde{b}^{sc}(t), \tilde{c}^{sc}(t)$  not only depend on  $\Delta/\epsilon_F$  and  $t \equiv T/T_{BG}$ , but also depend on  $\alpha$  in general.

The modification of  $\tilde{a}(t), \tilde{b}(t), \tilde{c}(t)$  by screening results in a modification of the AH conductivities. In Fig.2 of the main text, we show the difference of the AH conductivities with and without screening as a function of the rescaled temperature  $t \equiv T/T_{BG}$ . In the low temperature limit  $T \ll T_{BG}$ , we can expand  $\tilde{a}^{sc}(t), \tilde{b}^{sc}(t), \tilde{c}^{sc}(t)$  and get

$$\tilde{a}^{sc}(t) \approx \kappa \left( 1 + \pi^2 \frac{T^2}{T_{BG}^2} + \frac{51}{16} \pi^4 \frac{T^4}{T_{BG}^2} \right), \quad (106)$$

$$\tilde{b}^{sc}(t) \approx \kappa \left( 1 - 3\pi^2 \frac{T^2}{T_{BG}^2} - \frac{85}{16} \pi^4 \frac{T^4}{T_{BG}^2} \right), \quad (107)$$

$$\tilde{c}^{sc}(t) \approx \kappa \left( 1 - 7\pi^2 \frac{T^2}{T_{BG}^2} + \frac{323}{16} \pi^4 \frac{T^4}{T_{BG}^2} \right), \quad (108)$$

where  $\kappa \equiv \frac{\pi^2}{2\alpha^2} \frac{T^2}{T_{BG}^2} (1 - \Delta^2/\epsilon_F^2)$ .

The AH conductivities at  $T \ll T_{BG}$  with screening are then

$$\tilde{\sigma}_{xy}^{side}(\frac{\Delta}{\epsilon_F}, t) \approx -\frac{e^2}{4\pi \epsilon_F} \left( 1 - \frac{\Delta^2}{\epsilon_F^2} \right) \left[ 1 + \frac{17}{4} \pi^2 \left( 1 - \frac{\Delta^2}{\epsilon_F^2} \right) \frac{T^2}{T_{BG}^2} \right] \quad (109)$$

$$\tilde{\sigma}_{xy}^{sk-nc}(\frac{\Delta}{\epsilon_F}, t) \approx -\frac{17}{16} \pi e^2 \frac{\Delta}{\epsilon_F} \left( 1 - \frac{\Delta^2}{\epsilon_F^2} \right)^2 \frac{T^2}{T_{BG}^2}. \quad (110)$$

Comparing with the AH conductivities without screening in Table I of the main text, we can see that the AH conductivities are not changed by screening in the limit  $T \rightarrow 0$ . But at finite temperature, the screening modifies the AH conductivities as shown in the plots of Fig.2 in the main text.

At the high temperature limit  $T \gg T_{BG}$ , the AH conductivities depend on the TF wave vector for the screened case and there is no simple analytical result. The limiting values of the AH conductivities at  $T \gg T_{BG}$  also depend on  $\alpha$  and are different for the two cases with and without screening, as shown in the plots of Fig.2 in the main text.